Received: 4 June 2025 | Accepted: 2 December 2025

DOI: 10.1002/hem3.70292

ARTICLE

HemaSphere eha

IL21—STAT3 controls the pentose phosphate pathway to support metabolic reprogramming and tumor progression in chronic lymphocytic leukemia

Rosita Del Prete[1] | Vjola Tusha[1,2] | Helga Simon-Molas[3,4] | Virginia Anna Gazziero[1,5] | Federica Nardi[1] | Roberta Drago[1,6] | Gaia Bartolini[1] | Danilo Licastro[7] | Margherita Malchiodi[8] | Cristina Mariottini[8] | Giuseppe Marotta[9] | Giulio Caravagna[5,7] | Stefano Bruscoli[10] | Eric Eldering[3,4] | Alessandro Gozzetti[8] | Monica Bocchia[8] | Anna Kabanova[1]

Correspondence: Anna Kabanova (a.kabanova@toscanalifesciences.org)

Abstract

Studying how microenvironmental cues influence metabolic reprogramming can uncover mechanisms driving tumor progression. Using an in vitro model with proliferative stimuli of the in vivo lymph node niche (LN)—including interleukin-21 (IL-21)—we examined metabolic rewiring in chronic lymphocytic leukemia (CLL) cells. We found that the metabolic intermediates of upper glycolysis and its branching pathways are key in fulfilling metabolic demands of proliferating CLL cells. Among branching pathways, the pentose phosphate pathway (PPP) was the most transcriptionally upregulated in proliferating CLL cells. Increased expression of PPP genes was detected ex vivo at the bulk and single-cell level in the LN-resident and -emigrating CLL cells, with more consistency across enzymes of the nonoxidative PPP branch. Expression of the latter correlated with shorter failure-free survival in CLL patients. At the cellular level, metabolomics and 13C-glucose tracing confirmed high activity of the non-oxidative PPP in proliferating CLL cells. IL-21 regulated the expression of PPP enzymes, with STAT3 serving as the primary downstream effector. CRISPR/Cas9-mediated silencing of PPP enzymes revealed that, in vitro, proliferating CLL cells from most patients were not dependent on these enzymes. In contrast, silencing transketolase (TKT)—the rate-limiting enzyme of the non-oxidative PPP—abolished tumor engraftment in vivo, demonstrating that CLL cells rely on this pathway within the tumor microenvironment. These findings uncover a CLL-specific metabolic reprogramming wherein IL-21–STAT3 drives PPP activity and identify the nonoxidative PPP as a critical in vivo vulnerability of leukemic cells in the murine CLL model.

INTRODUCTION

The microenvironment can regulate tumor development through the direct control of its metabolism. One of the primary levels for such control is determined by the availability of essential nutrients. Beyond that, a wide array of stimuli present in the microenvironment could influence tumor metabolism through regulation of metabolic enzyme expression. This reprogramming may potentiate cellular fitness and proliferation capacity of tumor cells, but the implicated molecular mechanisms remain largely undefined. Filling this gap would offer new opportunities to understand tumor pathogenesis and manipulate tumor metabolism for therapeutic purposes.

[1]Fondazione Toscana Life Sciences, Siena, Italy
[2]PhD Program in Biotechnology, Department of Experimental Medicine and Biomedical Sciences, University of Perugia, Perugia, Italy
[3]Departments of Experimental Immunology and Hematology, Amsterdam University Medical Centers, Amsterdam, The Netherlands
[4]Amsterdam Institute for Infection and Immunity and Cancer Center Amsterdam, Cancer Immunology, Amsterdam, The Netherlands
[5]Department of Mathematics, Informatics and Geosciences, University of Trieste
[6]PhD Program in Translational and Precision Medicine, Department of Medical, Surgical and Neurosciences, University of Siena, Siena, Italy
[7]AREA Science Park, Padriciano, Trieste, Italy
[8]Hematology Unit, Department of Medicine, Surgery and Neurosciences, University of Siena, Siena, Italy
[9]Stem Cell Transplant and Cellular Therapy Unit, University Hospital of Siena, Siena, Italy
[10]Department of Medicine and Surgery, Section of Pharmacology, University of Perugia, Perugia, Italy

The tumor niche in malignancies that derive from mature B lymphocytes plays a special function in driving the transition of tumor B cells from quiescent to the activated and proliferative status. Similar transitions of cellular states occur in healthy B cells during the physiological immune response. In the context of chronic lymphocytic leukemia (CLL), the most frequent type of leukemia, tumor niche is represented by the bone marrow and lymph nodes (LN), through which malignant B cells from the peripheral blood continuously recirculate. The CLL cell pool in peripheral blood and the bone marrow is mostly quiescent, whereas the LN niche is enriched in activated and proliferating CLL cells.[1–5] The LN microenvironment provides CLL cells with mitogenic cues, contributing to their progressive expansion and playing a role in driving CLL resistance to therapy.[6–8] The changes of tumor cell metabolism driven by LN stimuli are hence expected to critically contribute to CLL pathogenesis.

LN-resident CLL cells show a transcriptional signature of cellular activation and clear signs of increased cellular proliferation in vivo.[1,9] In the LN proliferative niche, CLL cells are thought to be activated via B cell receptor signaling and by cell-to-cell interactions. $CD4^+$ T cells neighboring LN-resident CLL cells are acknowledged as major players promoting their proliferation, primarily through the stimulation of CD40 on the CLL cell surface.[10–12] T cells also release mitogenic cytokines. Among those, IL-21 has been detected in the CLL lymph node sections and is known to increase CD40-driven CLL cell proliferation in vitro.[11,13] Metabolic pathways regulated by these stimuli are still under investigation. Early steps of metabolic reprogramming promoted by the B cell receptor (BCR) and CD40 stimulation have been dissected previously, revealing changes in multiple branches of CLL cell metabolism.[12] However, metabolic rewiring and dependencies characterizing the late phases of CLL cell activation, coinciding with cellular proliferation, and the specific role of cytokines in CLL metabolism have not yet been studied.

In this study, we used an in vitro model with proliferative stimuli of the in vivo lymph node niche to dissect metabolic rewiring in proliferating CLL cells isolated from patients and the functional implication of such rewiring in tumor development. In this model, metabolite supplementation assays, RNA sequencing, ^{13}C-glucose isotope labeling, and metabolomics highlighted a prominent activation of the pentose phosphate pathway (PPP) during CLL cell proliferation. We identified that PPP is transcriptionally regulated through IL-21 and its downstream effector STAT3, representing a CLL-specific mechanism of metabolic reprogramming. Finally, by applying CRISPR/Cas9-mediated gene silencing to primary CLL cells, we demonstrate a role for PPP in supporting disease progression in vivo.

MATERIALS AND METHODS

Isolation and cryopreservation of human cells

Use of human samples was approved by the Comitato Etico Regionale per la Sperimentazione Clinica della Regione Toscana Area Vasta Sud Est (protocol TLS_LLC), and informed written consent was obtained. Additionally, 14 CLL patient samples were obtained from the B-cell malignancies Biobank of Amsterdam UMC, approved by the medical ethics committee of Amsterdam UMC under the registration number 2013-159. In this study, written informed consent was obtained from all subjects in accordance with the Declaration of Helsinki. Human B cells from CLL patients and healthy donors were isolated from peripheral blood by negative selection using the RosetteSep human B cell enrichment kit (StemCell) or from PBMCs using EasySep Human B cell enrichment kit II without CD43 depletion to >95% purity, in accordance with the manufacturer's instructions and after receiving signed informed consent according to the institutional guidelines. Cell freezing was performed according to a standard procedure. Briefly, cell pellets were gently resuspended in 10% DMSO/90% fetal bovine serum (FBS), transferred at −80°C in sealed polystyrene boxes, and then stored in liquid nitrogen until their usage. Cells were thawed by addition of warm medium and rapid shift to 37°C in a water bath, immediately centrifuged for 10 min at 200*g* to remove DMSO, and resuspended in medium for subsequent manipulation.

Proliferation assays with human CLL cells and healthy donor B cells

In most of the experiments, for which the use of physiological medium was required, B cells were cultured in HPLM (Thermo Fisher) with 10% dialyzed fetal bovine serum (dFBS, ECS0181L; Euroclone) and 50 µM 2-hydroxybutyric acid (2-HBA, A18636; Alfa Aesar) according to the manufacturer's instructions ("complete HPLM"). The following metabolites were supplemented to complete HPLM at working concentrations indicated in the Figure legends: fructose (F2543; Sigma-Merck), glucose (G7528; Sigma-Merck), inosine (I4125; Sigma-Merck), L-arginine (23 703; Cayman chemical), L-asparagine (A0884; Sigma-Merck), L-aspartic acid (A8949; Sigma-Merck), L-glutamine (49419; Sigma-Merck), L-isoleucine (I2752; Sigma-Merck), L-leucine (L8000; Sigma-Merck), L-methionine (M024; Chemodex), L-cystine (30200; Sigma-Merck), pyruvate (ThermoFisher, 11360), and uridine (Sigma-Merck, U3003). Culturing media used in Figure 1A are as follows: RPMI-1640 medium (Sigma-Merck) with 10% dFBS ("complete RPMI"); DMEM-high glucose medium (Sigma-Merck) with 10% dFBS; DMEM/F-12 medium (Thermo Fisher) with 10% dFBS; and IMDM medium (Sigma-Merck) with 10% dFBS. For cell viability and proliferation assays, 5×10^4 CLL cells/well were cultured for 5–6 days in a 96-multiwell tissue culture-treated plate (Greiner) with 6×10^3 irradiated hCD40L-expressing 3T3 feeder cells/well and a combination of 2.5 µg/mL F(ab')2 Fragment Goat Anti-Human IgM Fc5µ (Jackson Immunoresearch cat.n. 109.006.129), 10 ng/mL IL-4 (Immunotools), and 25 ng/mL IL-21 (Immunotools). For proliferation assays, B cells were pelleted by centrifugation at 110*g* for 10 min and incubated for 20 min in PBS-diluted 2.8 µg/mL CFSE (Thermo Fisher), quenched in FBS or complete RPMI at the end of incubation, and washed in PBS, as per the manufacturer's instructions. After 5–6 days of culturing, cell viability, total counts of live cells (reflecting cell expansion capacity), and CFSE dilution profiles were evaluated by flow cytometry using ZombieViolet viability dye (BioLegend). Data analysis was carried out with FlowJo v9.0 using the gating strategy presented in Supporting Information S1: Figure S1. For stimuli screening in Figure 7, CLL cells were cultured in complete HPLM with hCD40L-expressing 3T3 feeder cells, 2.5 µg/ml F(ab')2 Fragment Goat Anti-Human IgM Fc5µ and, as indicated, 100 U/mL IL-2, 10 ng/mL IL-4, 25 ng/mL IL-12, 25 ng/mL IL-15, or 25 ng/mL IL-21.

Glucose and NADPH/$NADP^+$ detection in the medium

Glucose detection in HPLM was performed using the glucose colorimetric assay kit (10009582; Cayman Chemical) according to the manufacturer's instructions. NADPH/NADP+ detection in human and mouse samples was performed using the luminescent assay kit (G9081; Promega) according to the manufacturer's instructions. Both assays were performed using as input 5×10^4 CLL cells/well cultured as indicated in Figure legends.

In vivo expansion and isolation of TCL1 cells

Primary Eµ-TCL1 B cells were kindly provided by the laboratory of Dr. Dimitar Efremov (International Center for Genetic Engineering

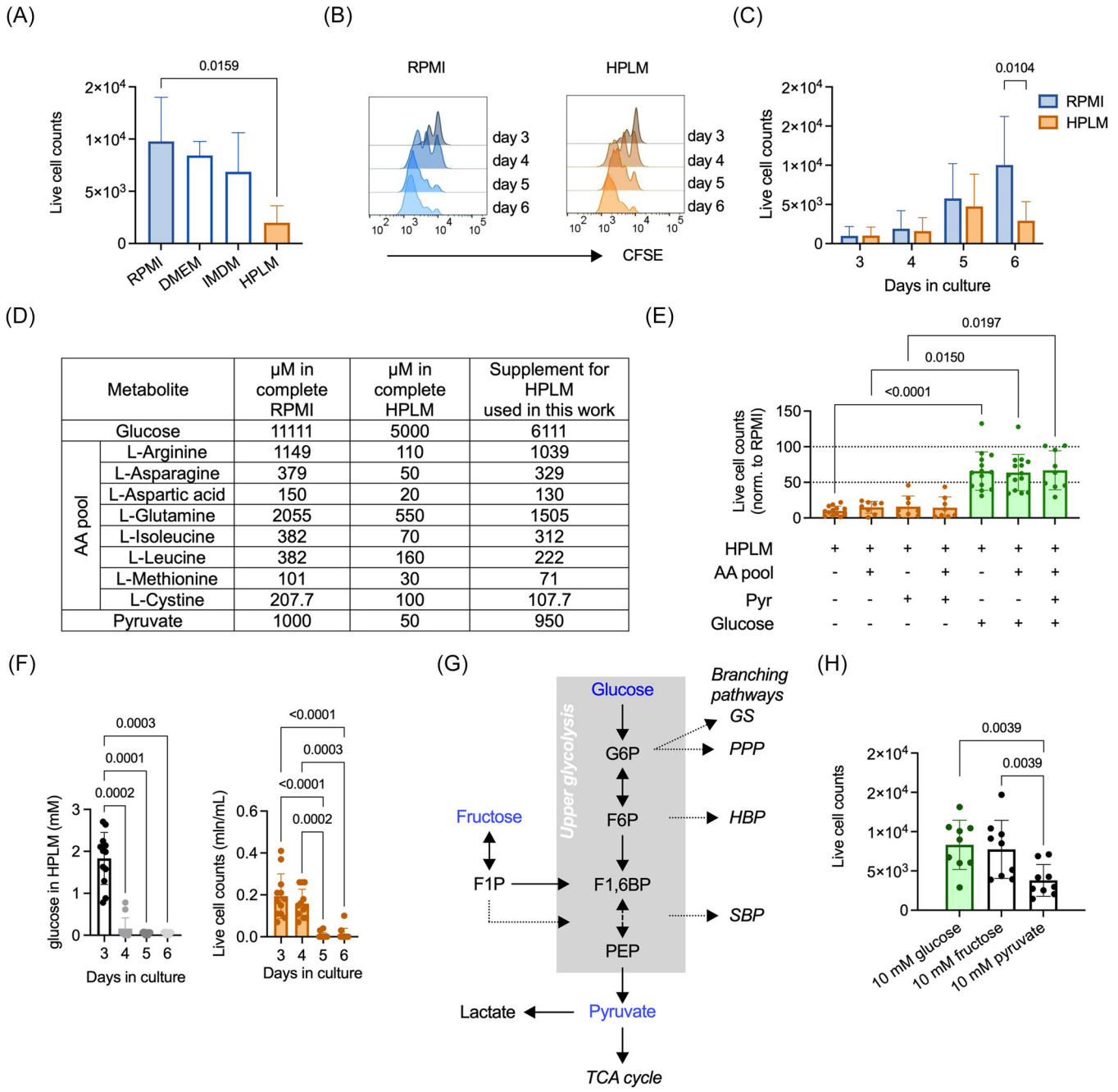

Metabolite		µM in complete RPMI	µM in complete HPLM	Supplement for HPLM used in this work
Glucose		11111	5000	6111
AA pool	L-Arginine	1149	110	1039
	L-Asparagine	379	50	329
	L-Aspartic acid	150	20	130
	L-Glutamine	2055	550	1505
	L-Isoleucine	382	70	312
	L-Leucine	382	160	222
	L-Methionine	101	30	71
	L-Cystine	207.7	100	107.7
Pyruvate		1000	50	950

FIGURE 1 **Survival of proliferating CLL cells is compromised by glucose shortage and is rescued by the intermediates of upper glycolysis and its branching pathways.** **(A)** Total counts of live CLL cells ($n = 3$ donors) cultured with irradiated CD40L-3T3 cells, αIgM (BCR-crosslinking) antibodies, IL-4, and IL-21 for 6 days in the media reported in the plot. *P* value 0.0159 was generated using the Mann–Whitney *U* test. **(B)** Representative CFSE profiling of CLL cells cultured for 3–6 days in RPMI or HPLM. **(C)** Daily total counts of live CLL cells ($n = 4$ donors) cultured for 3–6 days in RPMI or HPLM. The *P* value 0.0104 was generated using the Mann–Whitney *U* test. **(D)** Concentration of metabolites (µM) in complete RPMI and complete HPLM and their concentrations used for HPLM supplementation (experiments in panel **E**). AA pool, amino acid pool; Pyr, pyruvate. **(E)** Total counts of live CLL cells ($n = 7$–13 donors per condition) cultured for 6 days in HPLM or HPLM with supplement of the indicated metabolites (working concentrations reported in panel **D**). Cell counts were normalized to controls cultured in RPMI complete medium. *P* values were generated using the Kruskal–Wallis test. **(F)** Daily glucose detection in the culture medium (left panel) and counts of live cells (right panel) for CLL cells ($n = 12$ donors) cultured in HPLM. *P* values were generated using the Kruskal–Wallis test. **(G)** Schematic representation of glycolysis and the entry route of fructose into glycolysis. Solid arrows represent direct metabolic reactions; dashed arrows represent a series of reactions. Metabolite abbreviations: F1P, fructose 1-phosphate; F1,6BP, fructose 1,6-phosphate; F6P, fructose 6-phosphate; G6P, glucose 6-phosphate; PEP, phosphoenolpyruvate. Branching pathways: *GS*, glycogen synthesis; *HBP*, hexosamine biosynthesis pathway; *PPP*, pentose phosphate pathway; *SB*, serine biosynthesis; *TCA cycle*, tricarboxylic acid cycle. **(H)** Total counts of live CLL cells ($n = 9$ donors) cultured for 6 days in HPLM with the indicated supplement of metabolites. *P* values were generated using the Wilcoxon matched-pairs signed rank test. Bars represent the mean ± SD of the indicated individual values. Dots represent individual donors, or the mean value of technical replicates for each donor.

and Biotechnology, Trieste, Italy). Animal experiments were performed with necessary permissions from the Italian Ministry of Health (authorizations 578/2021-PR and 788/2023-PR). TCL1 cells were thawed in complete RPMI and centrifuged at 200*g* for 10 min. Then, cells were washed with PBS/3% FBS, centrifuged again, resuspended in PBS, and injected into wild-type female C57BL/6J recipients that were 7–8 weeks old ($5–10 \times 10^6$ TCL1 cells in 200 µL PBS i.v. 27 G syringe). Leukemia development was monitored by evaluating the percentage of CD5/CD19 double-positive cells in blood samples and by evaluating the enlargement of the spleen, weekly. Briefly, 3–4 drops of blood were collected and mixed with 10 µL of 0.5 M EDTA to avoid blood coagulation. A volume of 5 µL of blood was placed in a U-bottom 96 muti-well plate, previously saturated with 2% FBS in PBS. Next, 100 µL of ACK lysis buffer (8.29 g/L ammonium chloride, 1 g/L potassium bicarbonate, and 0.037 g/L EDTA) was used to lyse red blood cells (RBCs) on ice for 15 min. PBS (100 µL/well) was added to cells and centrifuged for 7–10 min at 800*g*. The pellet was washed with 200 µL of 2% FBS-PBS incubated with anti-mouse CD5 (cat.n. 100 608; Biolegend) and CD19 antibodies (cat.n. 115 512; Biolegend) on ice for 30 min. After incubation, cells were washed with 200 µL of 2% FBS-PBS and resuspended in 100 µL of PBS for flow cytometry analysis. For evaluation of spleen enlargement, mice were subjected to USG imaging using the VEVO 2100 Imaging System. Spleen volumes were calculated using the following formula: V_{spleen} (cm^3) = 0.0524 × width × length × thickness. In animals, after 50% of leukemic cells in blood were observed or the spleen volume became higher than 350–400 cm^3, their spleen was isolated and minced using a syringe plunger in PBS. Cell suspension was then passed through a 70 µm cell strainer and centrifuged for 10 min at 200*g*. The pellet was resuspended in 6 mL of PBS, carefully layered on the top of 6 mL of FicollPaque PREMIUM 1.084 (Cytiva), and centrifuged for 30 min at 500*g*. A splenocyte ring typically containing >90% TCL1 B cells was collected and resuspended in complete RPMI.

RNA sequencing and data processing

12×10^6 CLL cells/condition ($n = 4$ donors) were cultured in HPLM with 5 mM glucose in T-75 tissue culture-treated flasks (Greiner) with 1.4×10^6 of irradiated hCD40L-expressing 3T3 feeder cells/well, 2.5 µg/mL F(ab')2 Fragment Goat Anti-Human IgM Fc5µ (Jackson Immunoresearch cat.n. 109.006.129; Jackson Immunoresearch), 10 ng/mL IL-4 (Immunotools), and 25 ng/mL IL-21 (Immunotools). Controls were non-stimulated CLL cells lysed after cell thawing. After 4 days of culture, cells were collected, washed in PBS, stained with ZombieViolet (BioLegend) and anti-human CD19 antibody (cat.n. 302212; Biolegend), and sorted to collect viable $CD19^+$ CLL cells. Immediately after sorting, RNA was extracted using the NucleoSpin RNA extraction kit (Machery-Nagel). Extracted total RNA was quantitatively and qualitatively evaluated using NanoDrop 1000 (Thermo Fisher Scientific) and an Agilent Bioanalyzer 2100 (Agilent), respectively. RNA-seq libraries were prepared from 1 µg of total RNA with RIN 7-10, using the TruSeq® Stranded mRNA Library Prep (Illumina) according to the manufacturer's protocol. The resulting libraries were quality-checked for the insert size using a DNA 1000 Chip on Bioanalyzer 2100 (Agilent) and quantified using the Qubit™ dsDNA BR Assay Kit on a Qubit 2.0 Fluorometer (Thermo Fisher Scientific). Equimolarly pooled libraries were sequenced on the NovaSeq. 6000 Sequencing System (Illumina, Inc.) using 2 × 150 bp paired-end mode. Real-time image analysis and base calling were performed directly on the Novaseq instrument using the recommended sequencing control software. Illumina BCL2FASTQ v2.20 software (https://emea.support.illumina.com/downloads/bcl2fastq-conversion-software-v2-20.html) was used for de-multiplexing and production of FASTQ sequence files. FASTQ sequence files were subsequently quality-checked using FASTQC software (https://www.bioinformatics.babraham.ac.uk/projects/fastqc/). Subsequently, sequences with a low-quality score $Q < 20$, or those including only adaptor dimers, were discarded from the analysis. The resulting set of selected reads was aligned onto the complete human genome using STAR version 2.7.3 (Dobin and Gingeras, 2015) using hg38 Genome Assembly and Gencode.v35 as gene definition. The resulting Mapped reads were used as input for feature Counts function of Rsubread packages (https://bioconductor.org/packages/release/bioc/html/Rsubread.html). Differentially expressed genes were filtered using DESeq. 2 package in R (4.0.3)12 with default parameters. Raw read counts were used as input to generate the $\log_2$ fold changes, *P* values, and adjusted *P* values by applying default parameters. Differences in gene expression were considered significant for $P \leq 0.05$, adjusted $P \leq 0.1$, and $\log_2$ fold change > 1 or < −1. RNAseq data are available under accession number PRJNA973003.

Use of public RNAseq data sets

Figure 2C: Raw read counts from the published RNAseq data set GSE161711[14] from blood- and lymph node-derived sorted CLL cells ($n = 22$ donors) were analyzed to calculate FKPM values and[14] differentially expressed genes in DESeq. 2 package in R (4.0.3)12 with default parameters. Raw read counts were provided by Dr. Clare Sun (NIH National Heart, Lung, and Blood Institute) and used as input to generate the $\log_2$ fold changes, *P* values, and adjusted *P* values by applying default parameters. Differences in gene expression were considered significant for $P \leq 0.05$.

Figure 2E,F: Single-cell (sc)-RNAseq data representing peripheral blood-derived CLL cells from untreated donors were downloaded from two published studies.[15,17] For Nadeu et al., scRNA-seq expression matrices, Seurat objects (already filtered and clustered), and corresponding metadata were downloaded from https://doi.org/10.5281/zenodo.6631966; two donors (case 19 time point 3 and case 3299 time point 1) were analyzed. For Penter et al., raw counts, features, and barcodes matrices were downloaded from GSE165087 for samples and time points corresponding to the pre-treatment and high percentages of $CD19^+CD5^+$ cells (CLL1_3.1, CLL2_1, CLL3_1, CLL4_1, CLL5_1, CLL6_1, CLL7_1, and CLL8_1) were selected for the analysis. Samples were first scaled (each independently) and processed to filter low-quality cells and features. Further processing was performed with scripts and markers (*CD79A*, *CD3D*, *CD8A*, *IL7R*, *NKG7*, *LYZ*, *HBM*, *TOP2A*) released by Nadeu et al. in order to perform clustering, exclusion of non-B cells based on cluster markers, and annotation of *CXCR4highCD27low* and *CXCR4lowCD27high* clusters among B cell clusters. During these steps, samples in which CXCR4 and CD27 were not expressed were excluded, and clusters in which CXCR4 and CD27 were not differentially expressed were excluded from the analysis. Three cases from Penter et al. were finally retained (CLL2_1, CLL3_1, CLL6_1). The *FindMarkers* function from the Seurat package was used to run differential expression analysis between *CXCR4highCD27low* and *CXCR4lowCD27high* clusters for each donor.

Figure 2G and Supporting Information S1: Figure S4: Failure-free survival (FFS) and overall survival (OS) were analyzed on the RNAseq data set[16] derived from $n = 502$ CLL patients untreated at the time of sampling. RNAseq raw counts and clinical data were downloaded from https://cllmap.org. RNAseq counts were batch-corrected using the covariates reported in the original paper and the *combat_seq* function in the *sva* package, and then normalized using the DESeq. 2 variance stabilizing transformation function (*vst*). FFS and OS were

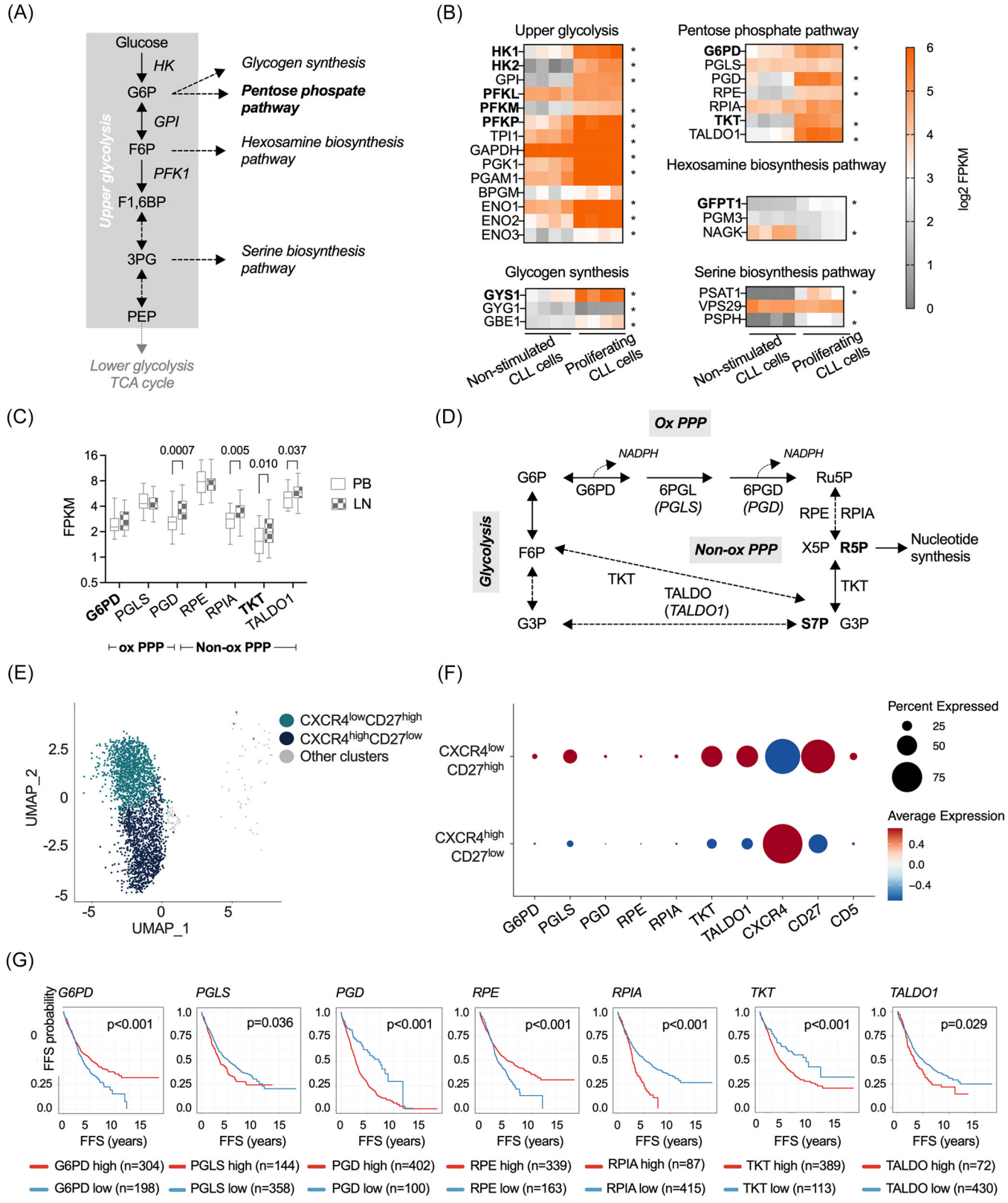

FIGURE 2 (See caption on next page).

FIGURE 2 **PPP enzyme expression and activity are upregulated in proliferating CLL cells.** **(A)** Schematic representation of glycolysis and glycolysis branching pathways. Solid arrows represent direct metabolic reactions; dashed arrows represent a series of reactions or the beginning of a glycolysis-related pathway. Metabolite abbreviations: 3PG, 3-phopshoglycerate; F6P, fructose 6-phosphate; F1,6BP, fructose 1,6-bisphosphate; G6P, glucose 6-phosphate; PEP, phosphoenolpyruvate. Enzyme abbreviations: *GPI*, glucose 6-phosphate isomerase; *HK*, hexokinase; *PFK1*, phosphofructokinase 1. **(B)** RNA sequencing data analysis showing enzymes of glycolysis and glycolysis-branching pathways expressed in proliferating CLL cells compared to nonstimulated cells. Cells were cultured for 4 days in HPLM with 5 mM glucose, CD40L-3T3 cells, αIgM (BCR-crosslinking) antibodies, IL-4, and IL-21 ($n = 4$ donors). Gene expression is reported as $\log_2$ FPKM for genes detected as expressed (mean $\log_2$ FPKM > 0). Differentially expressed genes (Table S2) are marked with asterisks. Rate-limiting enzymes of the pathways are highlighted in bold. **(C)** Expression values of PPP enzymes in $n = 22$ matched CLL cell samples sorted from the PB or the LN niche (LN).[14] Gene expression is reported as FPKM. Data are represented as box and whiskers depicting the median and min-to-max range of the individual values. *P* values were generated by DeSeq. 2. Rate-limiting enzymes of PPP branches are highlighted in bold. **(D)** Schematic representation of oxidative and nonoxidative branches of PPP. Solid arrows represent direct metabolic reactions; dashed arrows represent a series of reactions. Metabolite abbreviations: F1,6BP, fructose 1,6-biphosphate; F6P, fructose 6- phosphate; G3P, glyceraldehyde 3-phosphate; G6P, glucose 6-phosphate; R5P, ribose 5-phosphate; Ru5P, ribulose 5-phosphate; S7P, sedoheptulose 7-phosphate; X5P, xylulose 5-phosphate. Enzyme abbreviations: G6PD, glucose 6-phosphate dehydrogenase; 6PGL (*PGLS*), 6-phosphogluconolactonase; 6PGD (*PDG*), 6-phosphogluconate dehydrogenase; RPE, ribulose 5-phosphate epimerase; RPIA, ribulose 5-phosphate isomerase; TALDO (*TALDO1*), transaldolase; TKT, transketolase. **(E)** Uniform Manifold and Projection (UMAP) plot for PBMCs of case 19 from the published study[15] based on the scRNA-seq data colored by annotation. Only clusters expressing B cell markers are shown. **(F)** Expression of PPP genes in the two selected UMAP clusters identified in panel **(E)**. **(G)** Kaplan–Meier analysis of the impact of PPP enzyme expression on failure-free survival (FFS) in 502 treatment-naive patient samples.[16] FFS was calculated for treatment-naive patients as the time from the date of the sequenced sample to the date of first treatment, progression, or death, and censored at the last known event-free date. An independent analysis was performed for each gene. *P* values were generated using the log-rank test.

calculated for each gene independently for treatment-naive patients in the original study (ref). FFS was calculated as the time from the date of the sequenced sample to the date of first treatment, progression, or death, and censored at the last known event-free date; OS was calculated as the time from the date of the sequenced sample to the date of progression or death. Patients were classified as high/low for the expression of each PPP enzyme independently using the *surv_cutpoint* and *surv_categorize* functions from the *survminer* package (v 0.5.0). Survival analysis for each gene was then performed using the packages *survival* (v 3.8.3) and *ggsurvfit* (v 1.1.0), which were used also to construct Kaplan–Meier curves.

^{13}C-glucose isotope labeling analysis

A total of 12×10^6 CLL cells/condition ($n = 4$ donors) were cultured in HPLM with 5 mM glucose in T-75 tissue culture-treated flasks (Greiner) with 1.4×10^6 of irradiated hCD40L-expressing 3T3 feeder cells per flask, 2.5 µg/mL F(ab')2 Fragment Goat Anti-Human IgM Fc5µ (cat.n. 109.006.129; Jackson Immunoresearch), 10 ng/mL IL-4 (Immunotool), and 25 ng/mL of IL-21 (Immunotools). Controls were unstimulated CLL cells kept in the same culture medium for 24 h. After 4 days of culturing, cells were collected, centrifuged for 10 min at 200*g*, and washed in DMEM without glucose, glutamine, and phenol red (hereinafter named "blank DMEM," ThermoFisher, A1443001) and purified by density gradient centrifugation on Lympholyte Cell Separation media—Human (Euroclone, CL5020) in accordance with the manufacturer's instructions. Cells were resuspended at a density of 1×10^6/mL in blank DMEM with 0.55 mM glutamine (C0283; Sigma), 10% dFBS, and 9 mM D-Glucose-$^{13}C_6$ (CLM-1396; Cambridge Isotope Laboratories), and incubated at 37°C for 4 h. Then, cells were centrifuged as indicated above, washed in ice-cold 0.9% NaCl twice, pelleted, and stored at −80°C until the analysis. Samples were analyzed using a ZIC-cHILIC-based semi-targeted LC-MS platform following a liquid–liquid extraction in the presence of the internal standard Adenosine-$^{15}N_5$-monophosphate (5 nmol), as previously described.[12] Data were analyzed using Bruker TASQ software version 2.1.22.3. The relative isotope contribution was calculated using IsoCorrectoR Release 3.13.[18] Mean enrichment was calculated by adding the relative contribution of all isotopologues, except for M + 0, and represents the ^{13}C-labeled fraction of a given metabolite relative to the total amount of that metabolite within a sample. Total metabolite abundance was calculated by normalizing the corrected total abundance of each metabolite (all isotopologues, M + 0 included) by the cell number in each sample.^{13}C isotope labeling data will be made available via MetaboLights upon request to the corresponding author.

Immunoblotting

A total of 3×10^5 CLL cells or healthy donor B cells were cultured in a 24-multiwell plate (Greiner) for 3 days with 3.6×10^4 3T3-hCD40L feeder cells and with different soluble stimuli as indicated in the Figure legends. A total of 3×10^5 TCL1 B cells were cultured in a 24-multiwell plate (Greiner) for 3 days with 3.6×10^4 3T3-mCD40L feeder cells. Then, cells were filtered with a 40 µm strainer to remove feeder cells, centrifuged at 200*g* 10 min at room temperature, and resuspended in RIPA buffer. Cells were incubated for 5 min on ice and centrifuged at 200*g* for 10 min at 4°C. Supernatants were quantified using the BCA assay (Thermo Fisher). In total, 20 µg of total protein lysate was separated on 4%–12% polyacrylamide Bolt precast gels in MOPS SDS buffer (Thermo Fisher). Separated proteins were transferred to a PVDF membrane using the iBlot 2 dry blotting system (ThermoFisher) by applying an electric field of 20 V for 1 min, 23 V for 3 min, and 25 V for 2 min. The following antibodies were used for immunoblotting both human and mouse CLL cell lysates: rabbit anti-β-actin antibody (4967; Cell Signaling), rabbit anti-G6PD antibody (12263; Cell Signaling), rabbit anti-TKT antibody (64414; Cell Signaling), rabbit anti-STAT3 antibody (06-596; Upstate), and anti-rabbit IgG HRP (Jackson Immunoresearch). Band intensities of digital images were quantified by ImageJ software and normalized, first to the loading control (β-actin), and then to the control sample, which is indicated in the corresponding figure legends.

Electroporation of human and mouse B TCL1 cells with Cas9 RNPs

Sequences for synthetic 2′O-methyl/phosphothioate-modified sgRNAs (Synthego, Thermo Scientific, or Sigma-Aldrich) targeting human *CD4* and both mouse *Cd4* and *Tkt* were selected based on the optimal combination of specificity and efficiency scores predicted by the CRISPOR algorithms[19,20] (http://crispor.gi.ucsc.edu/); sequences for synthetic 2′ O-methyl/phosphothioate-modified sgRNAs targeting

human genes *G6PD*, *TKT*, and *STAT3* were derived from Synthego Gene Knockout Kit. SgRNAs were resuspended in RNAse-free 1xTE buffer (10 mM Tris pH 7.5–8.0, 1 mM EDTA) at 100 pmol/µL, aliquoted, and stored at −80°C. The sequences of the sgRNAs used are listed as follows:

Species	Gene ID	sgRNA	Exon
Human	*CD4*	GUCAGCGCGAUCAUUCAGCU	3
	G6PD	AGACGGUCGGGGGCAAGGCC	4
	G6PD	UCAUGUGGCUGUUGAGGCGC	4
	G6PD	CUUGAGCUUCUCCUCUGGGG	4
	TKT	CAGGAGCACUUACCGGGACC	3
	TKT	CAGGUUCAGCAGCUCCGCCU	3
	TKT	UGCAGCUCCCAUCCUCUACG	3
	STAT3	AAUCUUGACUCUCAAUCCAA	2
	STAT3	AGCUGUCACUGUAGAGCUGA	2
	STAT3	AUUUUAGCAGGAUGGCCCAA	2
Mouse	*Cd4*	CGGGUACCAGCCUGUUGCAA	4
	Tkt	AUCCAGGCCACCACCGCGGC	1
	Tkt	GCUUGCGGGAUGGCAUACAC	4

RNPs were formed by complexing 75 pmol recombinant Cas9 endonuclease (Integrated DNA technologies cat.n. 1081059; 10 mg/mL stock), 150 pmol sgRNAs, and 150 µg of poly-L-glutamic acid sodium salt (50,000–100,000 mw; Sigma) for 15–20 min at room temperature. For double sgRNA combination, the total sgRNA amount was maintained at 150 pmol per electroporation (75 pmol for each sgRNA). For each electroporation, $5–7 \times 10^6$ human B cells or 1×10^7 TCL1 cells were centrifuged at 800*g* for 10 min and washed in OptiMEM I medium (Thermo Fisher Scientific). After the second centrifugation, the pellet was resuspended in 100 µL OptiMEM/sample, to which the RNP complex was added. Cells were transferred into a 2 mm cuvette (EC-002; NepaGene) and electroporated on an NEPA21 electroporator (NepaGene). Next, 500 µL of complete medium was added to the cuvette and cells were then transferred into 2 mL of complete medium and counted. For cell expansion assays, $1–2 \times 10^4$ of live electroporated CLL cells/well were cultured in a 96-multiwell tissue culture-treated plate (Greiner) with 3×10^3 irradiated 3T3-hCD40L feeder cells/well. For human CLL cells, a cocktail of anti-human IgM/IL-4/IL-21 was added. For immunoblotting, the cultures were scaled up to a 24-multiwell plate format as indicated in the "immunoblotting" section. Silencing efficiency was evaluated by immunoblotting 3 days postsilencing, while viability and expansion/proliferation assays were performed 5 days postelectroporation at the DNA and protein levels.

Inference of CRISPR edits (ICE) analysis

5 days post-electroporation, $1–2 \times 10^6$ of Cas9 RNP electroporated cells were used to extract DNA using the Nucleo Spin Tissue kit (Macherey-Nagel). Genomic regions upstream and downstream of the cutting site were amplified for edited and non-edited control samples using the following primers:

Species	Gene ID	Forward primer	Reverse primer
Mouse	*Cd4*	GGTGGAGTTGTGGG TGTTCA	AGAGTGTCATGCCG AACCAG
	Tkt	CAGTCCTACCC AAGTCAGCC	ACACGTGCT CAGGTTTCTCC

Following Sanger sequencing, the ICE webtool[21] (https://ice.synthego.com/#/) was applied to estimate editing outcomes in terms of indel percentages with respect to the non-edited locus sequence.

In vivo transfer of *Cd4*- and *Tkt*-edited TCL1 cells

TCL1 cells were electroporated separately with single *Cd4*- or a combination of *Tkt*-targeting sgRNAs and cultured in complete RPMI with mCD40-3T3 irradiated feeder cells for 5 days. After ICE and immunoblotting validation of *Tkt* silencing, edited TCL1 cells were injected i.v. into wild-type 8-week-old female C57BL/6J mice (5×10^6 edited TCL1 cells in 200 µL PBS per animal) and leukemia that developed was monitored as described above. After splenocyte isolation as described above, a cell suspension was subjected to positive selection of CD19 cells using the EasySep Mouse CD19 Positive Selection Kit II (18954; StemCell) according to the manufacturer's instructions. The resulting suspension typically containing >95% $CD19^+$ cells was collected and resuspended in complete RPMI and used for subsequent experiments (DNA extraction and cell lysates).

Statistical analysis and software

Paired and not-paired nonparametrical statistical tests were applied, depending on the nature of the data to be analyzed. *P* values are indicated in Figure panels; statistical tests are indicated in Figure legends. Differences were considered significant when $P < 0.05$. GraphPad Prism version 10.1.1 for Windows (GraphPad Software) was used for the analysis.

RESULTS

Proliferating CLL cells depend on the metabolic intermediates of upper glycolysis and its branching pathways

Aiming to dissect the metabolic dependencies of proliferating CLL cells, we set up experiments culturing CLL cells for 5–6 days with a combination of "LN-like" stimuli, namely, 3T3 cells overexpressing human CD40L and soluble stimuli including antibodies to trigger the BCR, and cytokines IL-4 and IL-21, which, in combination, are known to maximize CD40-driven CLL cell proliferation.[13] First, we compared CLL cell expansion rates in different types of synthetic media, including the human plasma-like medium (HPLM), which was designed to contain glucose, amino acids, and small polar metabolites at levels similar to those in human plasma.[22,23] Compared to other media with supra-physiological metabolite concentrations, HPLM medium was not able to support CLL cell expansion in vitro (Figure 1A). CLL cells could proceed with cellular divisions in HPLM (Figure 1B), but after 5–6 days, they were dying (Figure 1C). This led us to hypothesize that some metabolites present in HPLM at lower concentrations compared to traditional media were rapidly depleted. We hence performed a metabolic rescue screen, wherein we supplemented HPLM with metabolites to reach the same concentration as that found in RPMI, focusing on metabolites that were at

least twofold less abundant in HPLM compared to other media (Figure 1D and Table S1). We found that supplementation with glucose, but not pyruvate or amino acids, was able to significantly increase the expansion of CLL cells in most of the samples analyzed, restoring it close to the levels of RPMI-cultured controls (Figure 1E). As expected, we found that glucose was rapidly consumed in HPLM cultures (Figure 1F, left panel), with increased mortality under glucose deprivation observed over time (Figure 1F, right panel).

Glucose-derived metabolites feed upper glycolysis, the associated branching pathways, and lower glycolysis, wherein pyruvate is converted into lactate and tricarboxylic acid (TCA) cycle intermediates (Figure 1G). To dissect the contribution of upper and lower glycolysis to the glucose dependency of proliferating CLL cells, we set up cultures with alternative carbon sources such as fructose and pyruvate. Fructose can enter glycolysis at the level of fructose 1,6-bisphosphate, feeding upper glycolysis and also the glycolysis branching pathways, whereas pyruvate in lower glycolysis can be converted into lactate or acetyl-CoA but cannot re-enter upper glycolysis or feed associated branching pathways (Figure 1G). Glucose and fructose supported CLL cell expansion more efficiently than pyruvate (Figure 1H). Our metabolic rescue experiments hence demonstrate that metabolites feeding upper glycolysis and its branching pathways might be particularly important in fulfilling the metabolic demands of proliferating CLL cells.

Expression of PPP enzymes, especially their nonoxidative branch, is upregulated in proliferating CLL cells and correlates with disease aggressiveness

To dissect rewiring of glucose metabolism during CLL cell proliferation, we performed RNA-seq analysis comparing nonstimulated and proliferating CLL cells and analyzed the expression of enzymes implicated in glycolysis and glycolysis-branching pathways, namely, the PPP, glycogen synthesis (GS), hexosamine biosynthesis (HBP), and the serine biosynthesis pathway (SBP) (Figure 2A). This analysis confirmed that most genes involved in these pathways were transcriptionally upregulated in proliferating CLL cells (25 out of 32 expressed genes; Figure 2B, and Table S2). PPP was the most highly upregulated glycolysis-branching pathway (FPKM mean fold change 4.02; Table S2) compared to GS and HBP, whereas we did not detect expression of the SBP rate-limiting enzyme phosphoglycerate dehydrogenase in most of the donors, indicating that it was probably inactive (Table S2).

To draw parallels between our in vitro model and the CLL proliferative niche in vivo, we compared expression levels of glucose metabolism-related enzymes pairwise between CLL cells sorted from the peripheral blood and patients' LNs from a previously published data set[14] (Figure S2). This ex vivo analysis revealed that PPP enzymes were upregulated in LN-resident CLL cells compared to the peripheral blood compartment (mean fold change 1.2) (Figure 2C and Table S2). PPP subdivides into the oxidative and non-oxidative branches, contributing, respectively, to the antioxidant NADPH production and de novo nucleotide synthesis[24] (Figure 2D). Interestingly, whereas only one enzyme of the oxidative PPP branch was upregulated in the LN-resident CLL cells (fold change *PGD* 1.45), most of the genes encoding enzymes of the non-oxidative PPP were upregulated (fold change *RPIA* 1.24, *TKT* 1.40, *TALDO1* 1.21; Figure 2C).

Additionally, we analyzed PPP enzyme expression in the two prominent subsets that could be identified in the peripheral CLL pool by single-cell (sc)-RNA sequencing. The CXCR4^{low}CD27^{high} subset defines pre-activated CLL cells that are expected to derive from recent LN emigrants and have a higher expression of another marker of the emigrants: CD5[25] (Figure 2E,F and Supporting Information S1: Figure 2S). The CXCR4^{high}CD27^{low} subset instead represents quiescent CLL cells, potentially ready to migrate toward the LN proliferative niche. Analysis of peripheral blood-derived cells from 5 CLL patients showed that most PPP enzymes are transcriptionally upregulated in the activated CXCR4^{low}CD27^{high} subset compared to the quiescent CXCR4^{low}CD27^{high} cells (mean fold change 1.48; Figure 2E,F, Supporting Information S1: Figure S3 and Table 2S), including *RPIA*, *TKT*, and *TALDO1*.

At the prognostic level, analysis of PPP enzyme expression performed in a large cohort of patients revealed that the levels of several PPP enzymes correlated with shorter failure-free survival (*PGD*, *RPIA*, *TKT*, *TALDO1*; Figure 2E and Table S3), whereas out of these genes, only *PGD* and *TALDO1* showed association with the overall survival (Supporting Information S1: Figure S4). Hence, our observations showed that transcriptional upregulation of PPP enzymes is a hallmark of CLL cells proliferating in vitro and originating from the LN proliferative niche ex vivo. Moreover, the levels of *RPIA*, *TKT*, and *TALDO1* of the non-oxidative PPP branch were consistently upregulated in all transcriptomics analyses and were predictive of CLL aggressiveness in terms of FFS.

The nonoxidative PPP branch is metabolically active in proliferating CLL cells

To analyze changes in the flux of glucose-derived carbons during CLL cell proliferation and, in particular, their flux through PPP, we performed ^{13}C-glucose isotope labeling analysis. Our results illustrated that glycolysis and its branching pathways are the primary metabolic pathways fed by glucose-derived carbons in proliferating CLL cells, since glucose-derived carbons were hardly incorporated into the TCA cycle (Supporting Information S1: Figure S4). In line with the transcriptomics results (Figure 2B), we found that proliferating CLL cells displayed active PPP, HBP, and lactate production, as ^{13}C carbons from glucose were detected in intermediates of all these pathways (Supporting Information S1: Figure S5), most of which displayed an increase in total amounts (Supporting Information S1: Figure S6). SBP was confirmed to be inactive (Supporting Information S1: Figure S4).

A closer look at PPP intermediates revealed a trend toward higher abundance for ribose-5-phosphate (R5P) in proliferating CLL cells (Figure 3A, left panel). No further enrichment of the fully labeled R5P (M + 5) fraction was observed in proliferating cells as compared to resting cells, indicating that the distribution of glucose-derived carbons in R5P was maintained (Figure 3A, right panel). Meanwhile, the total abundance of sedoheptulose-7-phosphate (S7P), a key metabolite of the nonoxidative PPP, was significantly upregulated in proliferating CLL cells (Figure 3B, left panel). The fraction of the fully labeled S7P isotopologue (M + 7) was also found to be increased in proliferating CLL cells compared to resting controls (Figure 3B, right panel), indicating higher synthesis of S7P directly from glucose-derived carbons. PPP intermediates contribute to the synthesis of nucleotides; in line with this, in proliferating CLL cells, there was also an enrichment in ^{13}C labeling of pyrimidine and purine nucleotides (uridine and adenosine in Figure 3C,D, left panels), paralleled by an increase in their total abundance (Figure 3C,D, right panels). Overall, these results illustrate that glucose-derived carbons actively feed PPP in proliferating CLL cells, with more prominent activity in the non-oxidative PPP branch.

IL-21 and STAT3 play a unique role in regulating the expression of PPP rate-limiting enzymes

Our in vitro model of CLL cell proliferation is based on the use of a combination of stimuli, including the CD40 ligand (CD40L), BCR-crosslinking antibodies, IL-4, and IL-21. In order to identify which

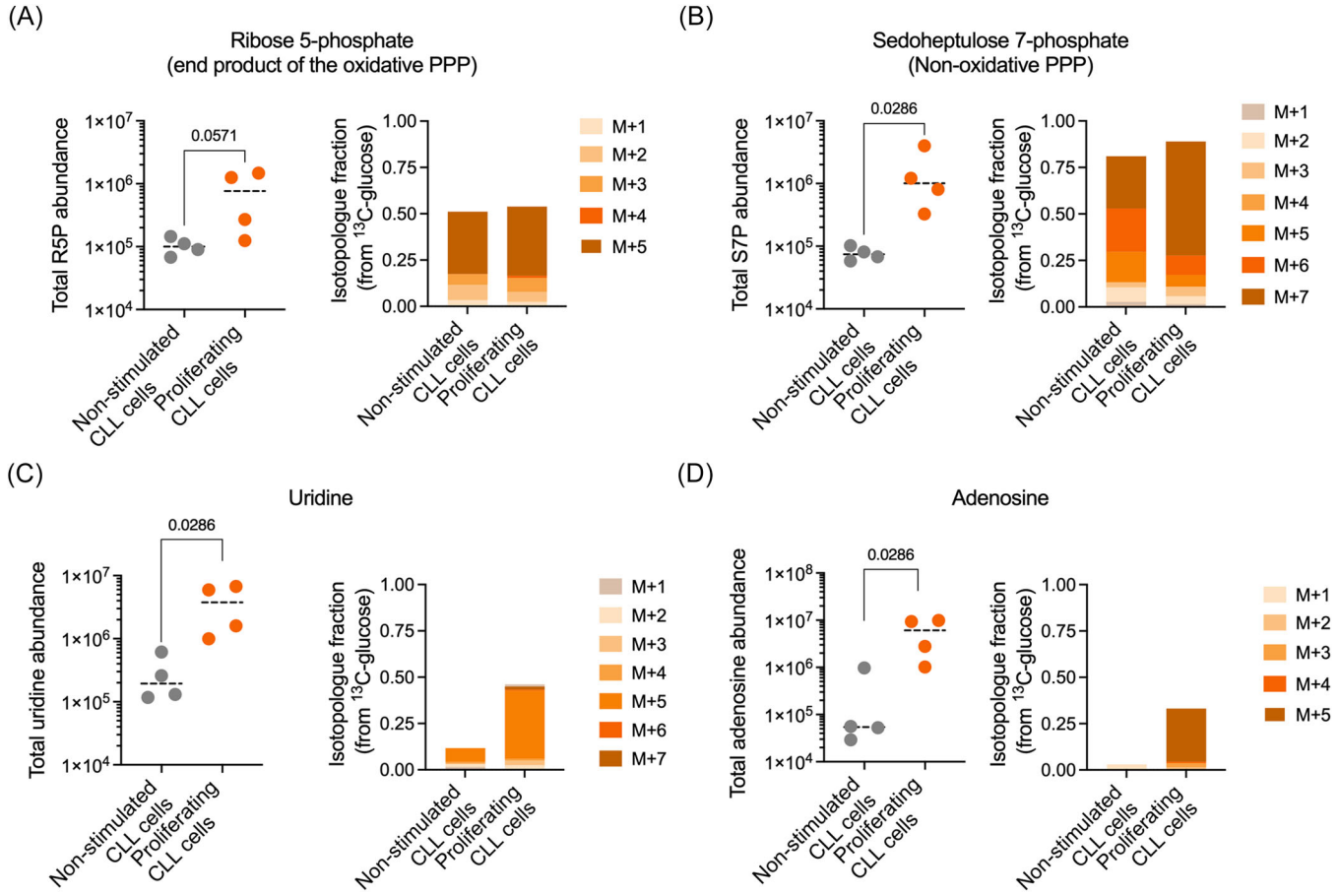

FIGURE 3 **^{13}C-glucose isotope labeling and metabolomics reveal the flux of glucose-derived carbons into PPP and nucleotide synthesis in proliferating CLL cells.** **(A)** Left panel: total metabolite abundance of R5P from ^{13}C-glucose isotope labeling data normalized by cell number. Right panel: distribution of R5P isotopologue forms (M + n) in ^{13}C-glucose tracing experiments. **(B)** Left panel: total metabolite abundance of S7P from ^{13}C-glucose isotope labeling data normalized by cell number. Right panel: distribution of S7P isotopologue forms (M + n) in ^{13}C-glucose tracing experiments. **(C)** Left panel: total metabolite abundance of uridine from ^{13}C-glucose isotope labeling data normalized by cell number. Right panel: distribution of uridine isotopologue forms (M + n) in ^{13}C-glucose tracing experiments. M + 8 and M + 9 forms were excluded from plotting (total abundance < 0.03). **(D)** Left panel: total metabolite abundance of adenosine from ^{13}C-glucose isotope labeling data normalized by cell number. Right panel: distribution of adenosine isotopologue forms (M + n) in ^{13}C-glucose tracing experiments. M + 6 to M + 10 forms were excluded from plotting (total abundance 0). Bars represent mean ± SD of the indicated individual values (n = 4 donors). P values were generated using the Mann–Whitney U test. Each dot represents one donor.

stimulus is responsible for the upregulation of PPP rate-limiting enzymes in proliferating CLL cells (Figure 2B), we assessed levels of G6PD and TKT in CLL cells treated with different stimuli or left resting. We observed that CD40L stimulation was able to promote weak upregulation of G6PD and TKT proteins compared to virtually null levels in resting CLL cells, while an addition of IL-21 to CD40L was able to significantly boost their expression (Figure 4A–D). IL-21 on its own was not able to mediate G6PD/TKT upregulation, indicating that synergy with CD40 stimulation is essential. This could be explained by the fact that CD40 stimulation is efficient in inducing the expression of the IL-21 receptor (IL21R), as indicated by transcriptomics data on CD40-stimulated CLL cells[12] (Figure 4E). Importantly, IL-21 boosted G6PD and TKT expression in combination with any type of stimulation, while the cocktail of CD40L, BCR-crosslinking antibodies, IL-4, and IL-21 yielded the highest expression levels of both PPP enzymes in all CLL donors tested (Figure 4A–D). The IL-21 boosting effect on G6PD and TKT expression was observed regardless of the mutational status of the *IGHV* immunoglobulin locus, the major molecular prognostic marker in CLL (Supporting Information S1: Figure S7A,B). Interestingly, in healthy B cells, as well as in roughly 20% of tested CLL donors, IL-21 did not exert a consistent boosting effect upon G6PD and TKT expression (Figure 4F–G; Figure S7C,D). Differential response to IL-21 was also found at the level of cell proliferation and in vitro expansion, since in healthy B cells, IL-21 did not promote an increase in CD40-driven proliferation, whereas it did so in CLL settings (Figure S8). This altogether suggested that IL-21, a T cell-derived cytokine that has been detected in the LN biopsies of CLL patients,[11] represents a CLL-specific stimulus promoting PPP reprogramming in the majority of CLL donors. IL-21 appears to play a distinct role in healthy B cells because it is not involved in the regulation of PPP enzyme expression, nor does it increase CD40-driven B cell proliferation.

To determine whether the role of IL-21 in inducing G6PD and TKT protein upregulation in combination with CD40L is unique or represents a general effect of cytokine addition, we tested various T cell-derived cytokines commonly used to induce CLL cell activation in vitro.[13,26–29] We found that, among various cytokines of the γ chain-binding family, only IL-21 was able to boost G6PD and TKT protein expression in CD40L-stimulated CLL cells (Figure 5A,B). Aiming to further dissect the mechanism of IL-21-mediated PPP

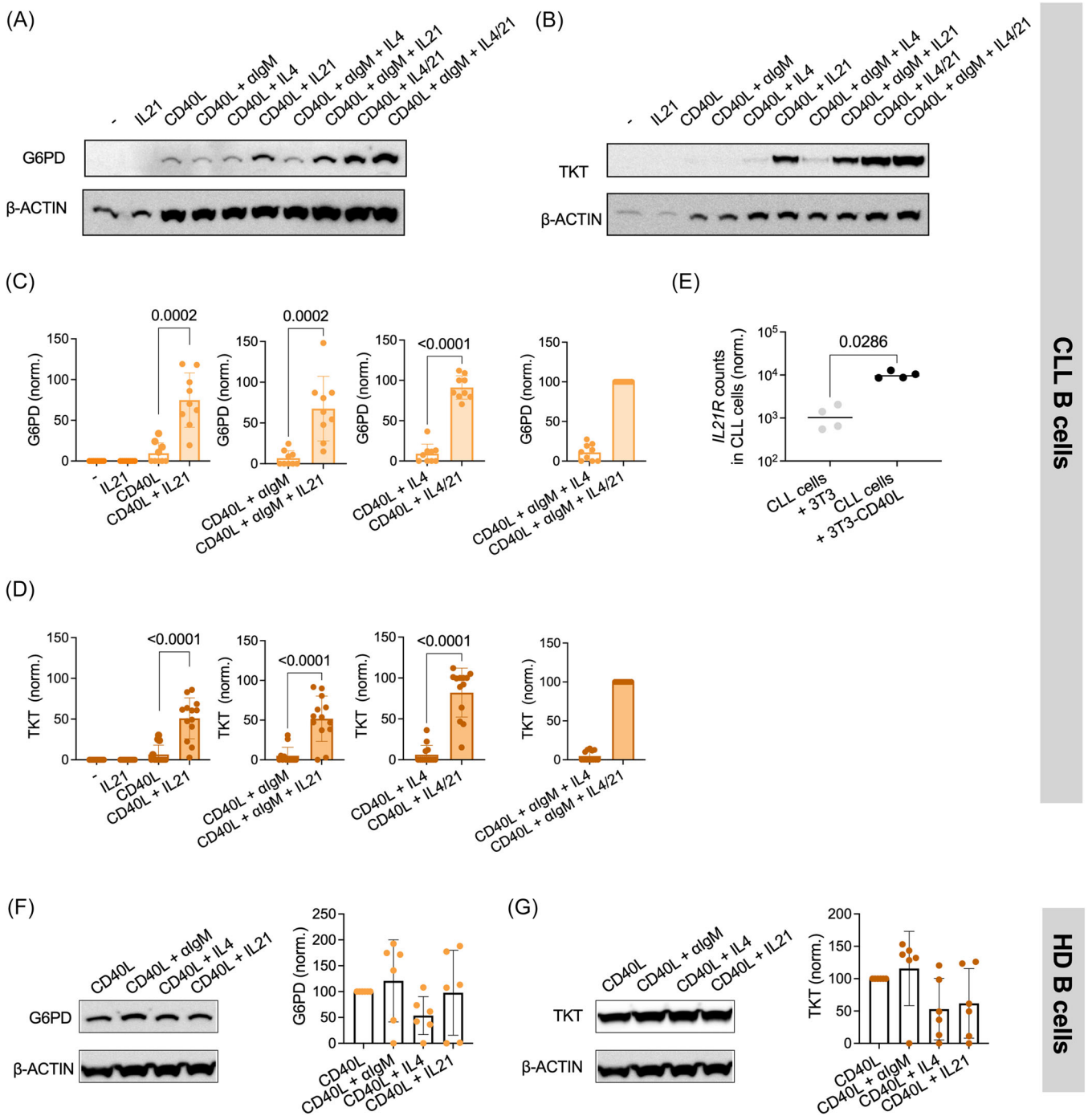

FIGURE 4 **IL-21 regulates the expression of G6PD and TKT in CLL cells but not in healthy B cells.** Representative immunoblots **(A)** for G6PD and for **(B)** TKT in primary CLL cells ($n = 9–13$ donors) stimulated for 3 days as indicated. "CD40L" denotes hCD40L-expressing 3T3 cells. **(C, D)** Quantification of immunoblots for G6PD and TKT in primary CLL cells ($n = 9–13$ donors) stimulated for 3 days as indicated. Data are normalized to the condition stimulated with CD40L, αIgM (BCR-crosslinking antibodies), IL4, and IL-21. **(E)** Analysis of *IL21R* expression from a published RNA sequencing analysis.[12] CLL cells were cultured for 48 h with 3T3 cells (Ctrl) or hCD40L-3T3 cells (CD40L). The *P* value was generated using the Mann–Whitney *U* test. **(F)** Example of an immunoblot (left panel) and quantification of immunoblots ($n = 6$ donors, right panel) detecting G6PD protein levels stimulated for 3 days with different stimuli combinations. In the right panel, data were normalized to the condition stimulated with CD40L. **(G)** Example of an immunoblot (left panel) and quantification of immunoblots ($n = 6$ donors, right panel) detecting TKT protein levels stimulated for 3 days with different stimuli combinations. In the right panel, data were normalized to the condition stimulated with CD40L. HD, healthy donor. Details of the clinical features of CLL donors are reported in Table S3. Data are represented as mean ± SD of the indicated individual values. *P* values were generated using the Mann–Whitney *U* test. Each dot represents one donor.

regulation, we evaluated whether the signal transducer and activator of transcription 3 (STAT3), a transcriptional factor that is one of the major effectors downstream of IL-21,[30] was implicated. We found that *STAT3* is transcriptionally upregulated during CLL cell expansion (Figure 5C). Interestingly, IL-21 was a positive regulator of STAT3 expression in proliferating CLL cells (Figure 5D,E, left panel). When we silenced *STAT3* using CRISPR/Cas9-mediated gene editing, the expression of both G6PD and TKT was reduced or ablated

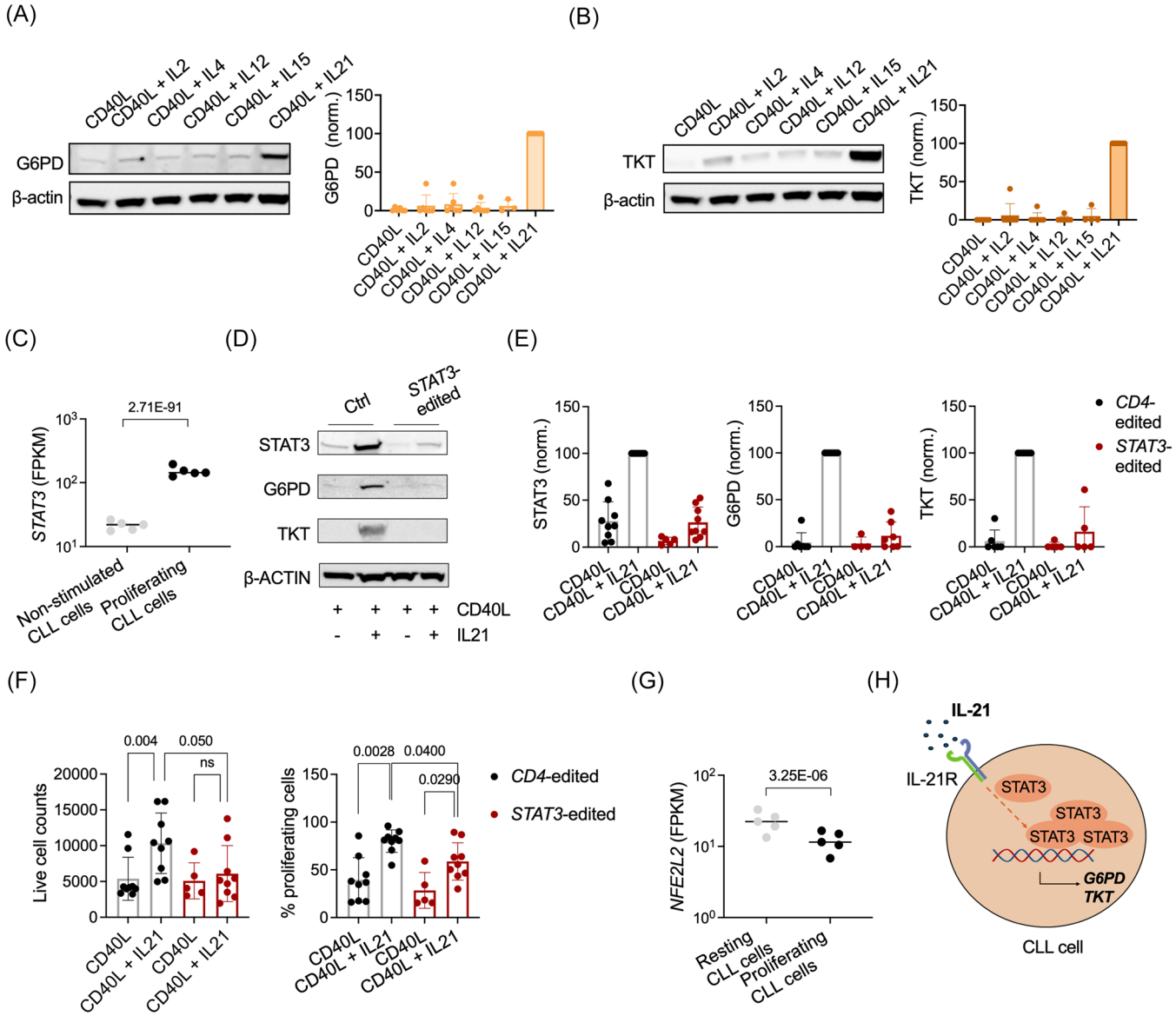

FIGURE 5 **Upregulation of G6PD and TKT expression occurs via the IL-21–STAT3 axis. (A)** Representative immunoblots (left panel) and their quantification (right panel) for G6PD in primary CLL cells ($n = 6$) stimulated for 3 days with different cytokines. "CD40L" denotes hCD40L-expressing 3T3 cells. **(B)** Representative immunoblots (left panel) and their quantification (right panel) for TKT in primary CLL cells ($n = 7$ donors) stimulated for 3 days with different cytokines. **(C)** RNA sequencing data analysis of *STAT3* in proliferating CLL cells compared to resting controls ($n = 5$ donors). The *P* value was generated by DeSeq. 2. **(D)** Representative immunoblots and **(E)** their quantification for STAT3, G6PD, and TKT in primary CLL cells ($n = 6–9$) stimulated for 3 days with different cytokines after *STAT3* silencing. *CD4*-edited cells were used as controls. Details of the clinical features of CLL donors are reported in Table S3. Data are represented as mean ± SD of the indicated individual values. **(F)** Total counts of live cells (left panel) and percentage of proliferating cells (right panel) in CLL cell cultures ($n = 5–9$ donors). Cells were genetically modified as reported in panels **(D, E)** and cultured with irradiated CD40L-3T3 cells, IL-4, and IL-21 for 5–6 days. *P* values were generated using the Mann–Whitney *U* test. **(G)** RNA sequencing data analysis of *NFE2L2* (encoding NRF2) in proliferating CLL cells compared to resting controls ($n = 5$ donors). The *P* value was generated by DeSeq. 2. **(H)** Graphical summary of IL-21-mediated regulation of STAT3 levels and PPP enzyme expression in CLL cells. Immunoblots **(A, B, E)** are normalized to the condition stimulated with CD40L and IL-21. Each dot represents one donor.

(Figure 5D,E, central and right panels), indicating a dependency of G6PD and TKT expression upon STAT3. This analysis also showed that the IL-21-mediated increase in CD40-driven CLL cell expansion, and to a lesser extent in the proliferation, was drastically diminished by *STAT3* silencing (Figure 5F). Interestingly, the known transcriptional activator of PPP enzyme expression, the nuclear factor erythroid 2-related factor 2 (NRF2 or *NFE2L2*), was downregulated during CLL proliferation, suggesting that it might not be implicated in the regulation of PPP enzymes in CLL settings (Figure 5G). Hence, our data suggest a novel regulatory mechanism wherein IL-21 amplifies its output through the upregulation of STAT3, which represents a major IL-21 downstream effector driving PPP enzyme expression and the increase in CD40-driven expansion of CLL cells (Figure 5H).

Expansion of CLL cells in vitro does not depend on the PPP enzymes G6PD and TKT in most patients

To evaluate whether PPP activity is essential for supporting the expansion of CLL cells in vitro, we opted for a genetic approach and

silenced rate-limiting enzymes of the pathway in primary leukemic cells via CRISPR/Cas9-based gene silencing.[31] Silencing efficiency reached 86.0 ± 11.3% in *G6PD*-edited CLL cells and 92.8 ± 9.2% in *TKT*-edited CLL cells at the protein level (Figure 6A,C). *CD4*-edited CLL cells were used as controls, as the *CD4* gene is not expressed in B cells. Analysis of in vitro expansion of CLL cells with silenced G6PD and TKT revealed variable behavior, with some samples displaying an increase and some displaying a decrease in cellular expansion (Figures 6B,D). Correlative analysis of cellular proliferation versus expansion revealed no significant relationship between the two measurements (Figure 6E,F). An arbitrary cut-off set to 35% inhibition of cell expansion indicated that 14.8% of samples with silenced *G6PD* and 31.3% of samples with silenced TKT had impaired in vitro expansion (Figure 6B,D). Distinction between the groups of patients with different dependency on the edited enzymes could not be linked to CLL clinical/prognostic factors (Supporting Information S1: Figure S9 and Table S3). Taken together, our data suggested that PPP enzyme silencing could exert a donor-dependent variable effect upon CLL cells, which was likely dependent on the differential survival of proliferating CLL cells rather than their proliferative capacity. Finally, we performed *G6PD* and *TKT* silencing in B cells derived from healthy donors (HDs) (Figure 6I,K). This analysis, performed on a limited number of samples, did not readily spot healthy B cells that were dependent on G6PD or TKT for their expansion in vitro (Figure 6J,L).

Next, we performed additional biochemical investigation of the role of PPP in CLL cell expansion. One of the important metabolic functions of the oxidative PPP branch is the G6PD-mediated production of NADPH (Figure 2D). We evaluated the impact of *G6PD* silencing on the production of NADPH in G6PD-independent CLL cells. We observed heterogeneous NADPH/$NADP^+$ ratios among different CLL samples and a decrease in the NADPH/$NADP^+$ ratio in *G6PD*-edited cells (Figure 6G). Since our data showed that cell expansion in most CLL donors did not depend on G6PD expression, we concluded that in most donors, NADPH production is not necessary to support metabolic needs of proliferating CLL cells. Another important metabolic function of both branches of PPP is to sustain de novo nucleotide synthesis.[32–35] We hence tested whether the supplementation of nucleotide precursors to cell culture media, which can replenish the nucleotide pool, would improve expansion of G6PD- and TKT-dependent CLL cells. Nucleoside addition promoted the expansion of most G6PD- and TKT-dependent CLL samples upon *G6PD* and *TKT* editing, respectively (Figure 6H), confirming that PPP activity contributes to nucleotide synthesis in proliferating CLL cells.

TKT silencing does not impact expansion of murine CLL cells in vitro but leads to the failure of tumor engraftment in vivo

To address the question of whether the activity of TKT in proliferating human CLL cells in vitro was relevant for CLL progression in vivo, we evaluated the effect of *Tkt* silencing in the widely used adoptive transfer Eμ-TCL1 mouse model.[36,37] Tkt was chosen as a target, since the nonoxidative PPP branch enzymes showed consistent upregulation in activated CLL cells in vitro and ex vivo (Figure 2B,C,E,F), while also displaying higher metabolic activity in proliferating CLL cells (Figure 3B). Primary leukemic TCL1 were genetically edited to silence TKT expression in the bulk tumor population using a CRISPR/Cas9-mediated approach (Figure 7A). *Tkt* silencing inhibited TCL1 cell expansion in vitro by only 19 ± 7.6% (Figure 7B). To assess the consequences of editing on leukemia development in vivo, we expanded *Tkt*-edited cells in vitro, transferred them into recipient animals, monitored leukemia development weekly, and analyzed gene editing in developed tumors (Figure 7C). This analysis was performed in two independent experiments and showed that mice injected with *Tkt*-edited cells displayed slower disease development, as measured by the accumulation of circulating $CD5^+CD19^+$ tumor cells in the blood, in comparison to their *Cd4*-edited counterparts (statistical significance reached in one of the experiments; Figure 7D). Accordingly, mice injected with *Tkt*-edited cells also showed slower spleen enlargement measured by ultrasonography (Figure 7E). When the percentage of leukemic cells in blood reached approximately 50% in the control group, all animals were killed. The initial level of TKT protein expression in the injected *Tkt*-edited cells was 21.2 ± 5.0%; however, this reverted to the control level in the developed tumors (Figure 7F,G). Validation of these results at the genetic level confirmed that *Tkt*-silenced TCL1 cells were lost during in vivo expansion, with the indel percentage at the *Tkt* locus being reset to zero in developed tumors (Figure 7H). At the same time, indel frequency in the *Cd4* locus in the control *Cd4*-silenced TCL1 cells and the corresponding tumors remained constant, indicating that the gene editing procedure itself did not lead to the loss of cell engraftment (Figure 7I). These results altogether suggest that *Tkt*-silenced cells show only moderate impairment in the ability to expand in vitro but are unfit in vivo and are rapidly outcompeted by the TKT-expressing wild-type tumor population, co-transplanted with the silenced one.

It is noteworthy that in the Eμ-TCL1 mouse model, IL-21 was not involved in the regulation of G6PD and TKT expression in proliferating TCL1 cells, suggesting that PPP is regulated differently in the mouse model compared to that in humans (Figure S10).

DISCUSSION

Our study illustrates that the IL-21–STAT3 axis regulates one of the essential branches of cellular metabolism, PPP, in a tumor-specific context. The relevance of this non-canonical mechanism to the pathogenesis of CLL, the most frequent type of leukemia, is supported by evidence collected on primary tumor cells from patients and the murine CLL model. We demonstrate that proliferating CLL cells reroute glucose-derived carbons into PPP and upregulate PPP enzymes in vitro and in the LN niche in patients. Silencing the rate-limiting PPP enzymes leads to patient-dependent variable outcomes in proliferating CLL cells. Only a minority of samples show dependence on PPP enzymes in vitro, which may be explained by differences in the metabolic flexibility of tumor cells across patients. Similarly, silencing of *Tkt* - the key rate-limiting enzyme of the nonoxidative PPP—did not significantly affect the expansion of murine CLL cells in vitro. However, *Tkt* appears to be necessary to support tumor cell engraftment in vivo. Our results therefore suggest that PPP becomes functionally important in the physiological tumor niche.

Previous studies proposed mitochondrial metabolism as a key metabolic feature in activated CLL cells[12,38] and in proliferative and clinically aggressive CLL.[39] Mitochondrial metabolism in CLL cells is fueled by glutamine, without evident contribution from glucose,[38] which was confirmed by us in proliferating CLL cells also in this study. Our findings point to PPP as another key metabolic rewiring in CLL by providing evidence of the redirection of glucose-derived metabolites into nucleotide synthesis. This altogether suggests that both glucose- and glutamine-driven metabolic pathways play non-redundant and important roles in CLL biology.

Our data suggest that the non-oxidative branch of PPP is particularly active in proliferating CLL cells. Supporting the physiological relevance of this finding, transcriptomics of tumor cells residing in or originating from the LN proliferative niche reveal a consistent

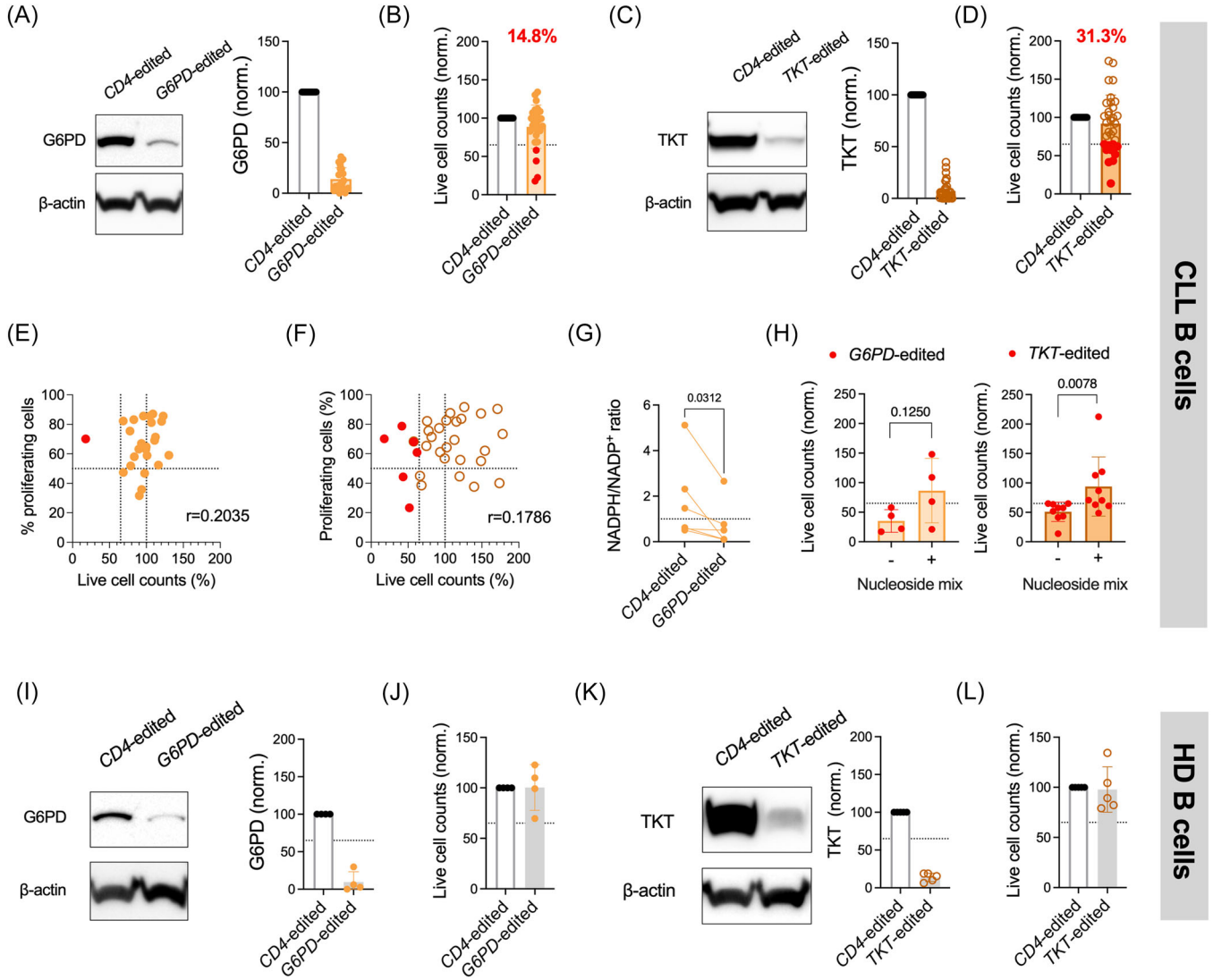

FIGURE 6 **Expression of the PPP enzymes G6PD and TKT is critical and functionally important for in vitro CLL cell expansion in a subset of CLL donors. (A)** Representative G6PD immunoblots (left panel) and their quantification (right panel) for *CD4*- and *G6PD*-edited CLL cells ($n = 27$) cultured for 5 days in HPLM with 5 mM glucose. **(B)** Total counts of live *G6PD*-edited CLL cells ($n = 27$) normalized to *CD4*-edited controls. CLL cells were cultured for 5 days in HPLM with 5 mM glucose. G6PD-dependent donors are highlighted in red ($n = 4$). **(C)** Representative TKT immunoblots (left panel) and their quantification (right panel) of *CD4*- and *TKT*-edited CLL cells ($n = 32$) cultured for 5 days in HPLM with 5 mM glucose. **(D)** Total counts of live *TKT*-edited CLL cells ($n = 32$) normalized to *CD4*-edited controls. CLL cells were cultured for 5 days in HPLM with 5 mM glucose. TKT-dependent donors are highlighted in red ($n = 10$). **(E)** Correlative analysis between total counts of live *G6PD*-edited cells and percentage of proliferating cells among live *G6PD*-edited cells ($n = 25$ donors). *r*, Pearson coefficient. **(F)** Correlative analysis between total counts of live *TKT*-edited cells and percentage of proliferating cells among live *TKT*-edited cells ($n = 31$ donors). *r*, Pearson coefficient. **(G)** Detection of the NADPH/$NADP^+$ ratio in *G6PD*-independent CLL cells ($n = 5$) after *G6PD*-silencing. The *P* value was generated using the Wilcoxon matched-pairs signed rank test. **(H)** Total counts of live *G6PD*-silenced CLL cells from G6PD-dependent donors ($n = 4$, left panel) and *TKT*-silenced CLL cells from TKT-dependent donors ($n = 9$, right panel). CLL cells were cultured for 5 days in HPLM supplemented with 5 mM glucose, with or without nucleoside mixture (1 mM uridine, 1 mM inosine). Total counts were normalized to *CD4*-edited controls cultured in HPLM supplemented with 5 mM glucose. *P* values are generated using the Wilcoxon matched-pairs signed rank test. **(I)** Representative G6PD immunoblots (left panel) and their quantification (right panel) in *CD4*- and *G6PD*-edited healthy donor (HD) B cells ($n = 5$) cultured for 5 days in HPLM with 5 mM glucose. **(J)** Total counts of live *G6PD*-edited healthy B cells ($n = 5$) normalized to *CD4*-edited controls. B cells were cultured for 5 days in HPLM with 5 mM glucose. **(K)** Representative TKT immunoblots (left panel) and their quantification (right panel) in *CD4*- and *TKT*-edited healthy B cells ($n = 5$) cultured for 5 days in HPLM with 5 mM glucose. (L) Total counts of live *TKT*-edited healthy B cells ($n = 5$) normalized to *CD4*-edited controls. B cells were cultured for 5 days in HPLM with 5 mM glucose. Data are represented as mean ± SD of the indicated individual values. Each dot represents one donor.

upregulation of most enzymes of the non-oxidative PPP branch. Moreover, expression of these enzymes correlates with shorter FFS in patients. Non-oxidative PPP remains relatively understudied in the field of cancer and immune cell metabolism, while in the field of blood cancer, it has not been studied at all.[24] Several studies have described the role of the TKT in solid tumors through its promotion of tumor aggressiveness, metastasis, drug resistance,[40–42] and redox-related function.[43–47] Hence, TKT has been proposed as a potential therapeutic target, in line with our data on its essential role in CLL engraftment in vivo. So far, TKT targeting has been explored only at the preclinical level. The anti-metabolite oxythiamine has been used for TKT targeting both in vitro[48] and in vivo.[43] However, this

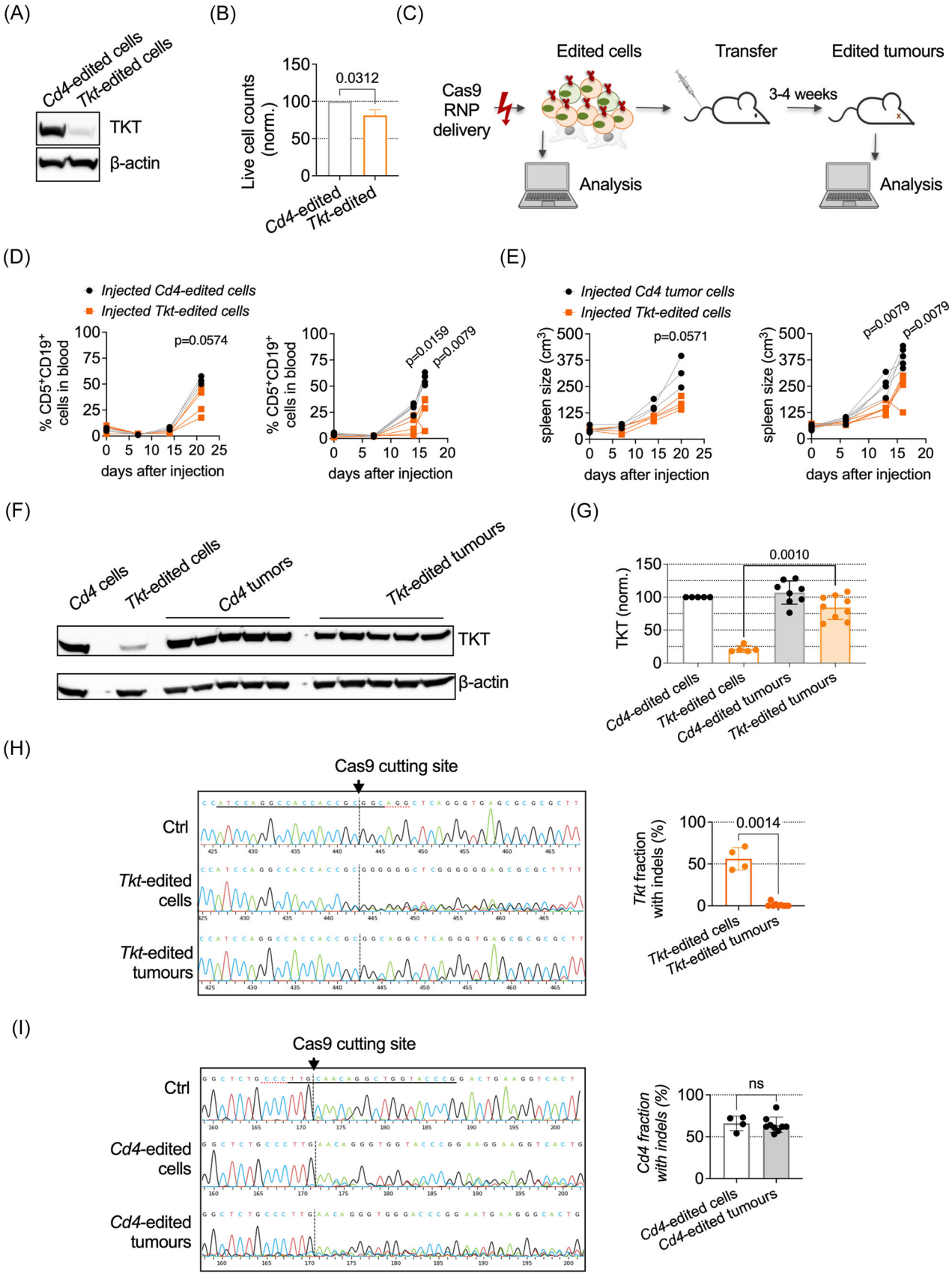

FIGURE 7 (See caption on next page).

FIGURE 7 **TKT silencing results in the loss of CLL cell fitness and delay of leukemia progression in vivo.** **(A)** Representative immunoblot of TKT in *Cd4*-edited and *Tkt*-edited TCL1 cells cultured for 4 days. **(B)** Total counts of live *Cd4*-edited and *Tkt*-edited TCL1 cells expanded in vitro in co-cultures with irradiated CD40L-m3T3 cells for 5 days. **(C)** Workflow of transfer experiments in which CRISPR/Cas9-based edited TCL1 cells are injected into a healthy recipient and analyzed before and after their transfer. **(D)** Percentage of $CD5^+CD19^+$ leukemic cells in the blood of mice injected with *Cd4*-edited ($n = 8$ mice) and *Tkt*-edited TCL1 cells ($n = 9$ mice). Results display two independent experiments (left and right panels, respectively). Each dot represents one animal. **(E)** Measurements of spleen size in mice injected with *Cd4*-edited ($n = 8$ mice) and *Tkt*-edited TCL1 cells ($n = 9$ mice). Results display two independent experiments (left and right panels, respectively). Each dot represents one animal. **(F)** Representative immunoblot and **(H)** quantification of TKT levels in *Cd4*- and *Tkt*-edited TCL1 cells before injection, and in the corresponding tumors. Each dot represents one animal. **(I)** Representative Sanger sequencing histograms of an amplified *Tkt* locus in edited TCL1 cells and resulting tumors (left panel). Indel frequency in the *Tkt* locus based on *Inference of CRISPR* editing (ICE) analysis (right panel). Each dot represents one animal. **(H)** Representative Sanger sequencing histograms of an amplified *Cd4* locus in edited TCL1 cells and resulting tumors (left panel). Indel frequency in the *Cd4* locus based on *Inference of CRISPR* editing (ICE) analysis (right panel). The Cas9 cutting site is indicated and the *Tkt* sgRNA sequence is underlined. Each dot represents one animal. Data in the figure represent mean ± SD of the indicated individual values. In panels **(B**, **C**, **D**, **F**, **G**, and **H)**, *P* values were generated using the Mann–Whitney *U* test.

anti-metabolite could potentially inhibit other thiamine-dependent enzymes[49] and hence might lack specificity. A new specific TKT inhibitor, oroxylin A, has been recently identified.[50] Since no extensive preclinical or clinical studies with oroxylin A or any other TKT targeting compounds have been conducted so far, investing research efforts into this area represents the logical next step, based on the evidence that we have provided in this study. Furthermore, TKT inhibitors could be exploited in combination with current CLL therapies, in view of the promising in vitro data suggesting that mitochondrial metabolism inhibition can counteract resistance to Bcl2 inhibitors.[38]

In addition to exploring the role of TKT, we also studied the role of G6PD, which is the rate-limiting enzyme of the oxidative PPP branch. Our data showed that *G6PD* is not among the enzymes upregulated in CLL cells in the LN niche in vivo. Moreover, its silencing is associated with a decrease in intracellular NADPH levels, which, however, affects CLL cell expansion in vitro only modestly. This is an unexpected result, given that G6PD plays an important redox-protective function in tumor cells of B cell acute lymphoblastic leukemia (B-ALL).[51] We hypothesize that differences in dependency upon G6PD in B-ALL and CLL could be potentially linked to differences that one might expect between immature and mature B cells representing the cell of origin for B-ALL and CLL, respectively.

At the mechanistic level, one of the key findings of this study is that expression of PPP enzymes is regulated by IL-21 and STAT3. Previously, the transcription factor NRF2, which activates the transcription of cytoprotective genes and thus orchestrates the oxidative stress sensor pathway, has been described as a key regulator of PPP enzyme expression.[52] Our study demonstrates instead that, in CLL settings, PPP is controlled via a cytokine-driven STAT3 axis, albeit the observed dependence on STAT3 was partial for some of the investigated samples, suggesting potential involvement of NRF2 or other factors yet to be established. This finding provides a new mechanistic insight into the role of IL-21 and STAT3 in CLL biology. IL-21 has been detected in tumor proliferation centers in the CLL lymph nodes.[11] IL-21 acts synergistically with CD40 to promote CLL cell proliferation in vitro[11] and increase the engraftment of patient-derived CLL xenografts in vivo.[53] Interestingly, in the broader context of B cell biology where the role of IL-21 has been widely studied, no aspects related to the regulation of metabolism have been described. Instead, we found IL-21 to be dispensable for G6PD and TKT expression in CD40-stimulated healthy B cells, suggesting that there are substantial differences in the regulation of PPP between leukemic and healthy B cells. We also observed that other cytokines of the γ_c family that are interchangeably used in different studies to induce activation of CLL cells in vitro, such as IL-2,[54] IL-4,[13,28] or IL-15,[27,29] fail to induce TKT and G6PD upregulation. This indicates that the choice of cytokines may alter the CLL cell phenotype significantly and should be taken into consideration for the setup of in vitro assays.

STAT3 has been previously studied in CLL, mostly in quiescent cells from peripheral blood, where STAT3 appears to be constitutively active[55] and contributes to the expression of immunomodulatory genes such PD-L1, IL-10, and pentraxin 3.[56,57] Pharmacological inhibition of STAT3 by the small molecule pyrimethamine impaired CLL cell viability,[58] suggesting that it could be a druggable target. A clinical phase I trial with pyrimethamine administered to CLL patients with extensive prior history of treatments showed that, although no objective responses were documented, 50% of patients in the study achieved stable disease.[58] Altogether, this reinforces the concept of STAT3 implication in CLL pathogenesis. From a metabolic point of view, the role of STAT3 has not been explored in B cells, but only in other cell types. For instance, in healthy tissues, STAT3 was shown to potentiate mitochondrial function, supporting the electron transport chain[59] and TCA cycle activity,[60] whereas in chronic myeloid leukemia, STAT3 appears to dysregulate mitochondrial metabolism, promoting a shift toward glycolysis.[61] Hence, metabolic outputs of STAT3 activity seem to vary considerably between different cell types.

Altogether, this complexity highlights the need to map downstream effectors of STAT3-driven transcriptional programs in a cell type-dependent manner. This could pinpoint new regulatory mechanisms in the pathogenesis of each tumor, specifically including those responsible for metabolic reprogramming. Our study illustrates that, in proliferating CLL cells, the activity of PPP activity is regulated via the IL-21–STAT3 axis and that specifically the non-oxidative PPP branch is essential for tumor cell fitness in the murine CLL model in vivo. Other regulatory nodes of the STAT3 program or metabolic cues beyond IL-21 implicated in the metabolic reprogramming in CLL await identification, and their targeting might hold therapeutic promise.

ACKNOWLEDGMENTS

The authors would like to thank Drs Dimitar Efremov and Supriya Chakraborthy (International Centre for Genetic Engineering and Biotechnology, Trieste, Italy) for providing TCL1 leukemic clones and hCD40L-3T3 cells, and for in-depth discussions; Silvia Valensin, Antonella De Rosa, Erika Bellini, and Davide Bosco (Fondazione Toscana Life Sciences, Siena, Italy) for technical assistance with in vivo experiments; Simona Tavarini and Chiara Sammicheli (GlaxoSmithKline Vaccines, Siena, Italy) for cell sorting and assistance with flow cytometry; Dr. Małgorzata Firczuk (Mossakowski Medical Research Institute Polish Academy of Sciences, Warsaw, Poland) and Dr. Andrea Brendolan (San Raffaele Scientific Institute, Milan, Italy) for providing technical tips on the TCL1 model; Dr. Mark Connors (National Institute of Allergy and Infectious Diseases, US) for the generous gift of mCD40L-3T3 cells; the Core Facility Metabolomics (Amsterdam UMC, University of Amsterdam, Meibergdreef 9, 1105

AZ Amsterdam, the Netherlands) for analyzing 13C-glucose isotope labeling data; Dr. Arnon Kater (Amsterdam UMC, University of Amsterdam) and Dr. Julie Dubois (Biobank & Central Lab – B cell malignancies, BeBo Lab - Bloed en Beenmerg Onderzoek, Amsterdam UMC) for providing CLL clinical samples; and Dr. Clare Sun (NIH National Heart, Lung and Blood Institute) for providing RNAseq data set details.

AUTHOR CONTRIBUTIONS

Rosita Del Prete: Writing—original draft; writing—review and editing; investigation; validation; formal analysis; supervision; visualization; methodology. **Vjola Tusha**: Investigation; validation; formal analysis; visualization; writing—review and editing. **Helga Simon-Molas**: Investigation; formal analysis; data curation; writing—review and editing. **Virginia Anna Gazziero**: Data curation; software; visualization. **Federica Nardi**: Investigation; data curation. **Roberta Drago**: Investigation. **Gaia Bartolini**: Investigation. **Danilo Licastro**: Resources. **Margherita Malchiodi**: Resources. **Cristina Mariottini**: Resources. **Giuseppe Marotta**: Resources. **Giulio Caravagna**: Supervision; data curation. **Stefano Bruscoli**: Supervision; writing—review and editing. **Eric Eldering**: Writing—review and editing. **Alessandro Gozzetti**: Resources; supervision. **Monica Bocchia**: Resources; supervision. **Anna Kabanova**: Conceptualization; funding acquisition; writing—original draft; writing—review and editing; project administration; supervision; formal analysis; visualization.

CONFLICT OF INTEREST STATEMENT

The authors declare no conflict of interest.

DATA AVAILABILITY STATEMENT

The data that support the findings of this study are openly available in NCBI at https://www.ncbi.nlm.nih.gov/bioproject/PRJNA973003/, reference number PRJNA973003.

Sequencing data generated in this study are publicly available in Gene Expression Omnibus (GEO) PRJNA973003.^{13}C isotope labeling data were generated at the facility of the Amsterdam University Medical Centers and will be made available upon request to the corresponding author.

FUNDING

RDP acknowledges support from the AIRC Foundation for Cancer Research (postdoctoral fellowship Michele e Carlo Ardizzone, ID 26636-2021). AK acknowledges support from the AIRC Foundation for Cancer Research (My First AIRC grant 21495) and the European Union–NextGenerationEU through the Italian Ministry of University and Research under PNRR–M4C2-I1.3 Project PE_00000019 "HEAL ITALIA," CUP B63D22000680006. The views and opinions expressed are those of the authors only and do not necessarily reflect those of the European Union or the European Commission. Neither the European Union nor the European Commission can be held responsible for them.

SUPPORTING INFORMATION

Additional supporting information can be found in the online version of this article.

ORCID

Virginia Anna Gazziero https://orcid.org/0009-0008-3024-1039
Alessandro Gozzetti https://orcid.org/0000-0003-0769-6891
Anna Kabanova https://orcid.org/0000-0002-2077-472X

REFERENCES

1. Herishanu Y, Pérez-Galán P, Liu D, et al. The lymph node microenvironment promotes B-cell receptor signaling, NF-κB activation, and tumor proliferation in chronic lymphocytic leukemia. *Blood*. 2011;117(2):563-574. doi:10.1182/blood-2010-05-284984
2. Cuthill KM, Zhang Y, Pepper A, et al. Identification of proliferative and non-proliferative subpopulations of leukemic cells in CLL. *Leukemia*. 2022;36(9):2233-2241. doi:10.1038/s41375-022-01656-4
3. Herndon TM, Chen SS, Saba NS, et al. Direct in vivo evidence for increased proliferation of CLL cells in lymph nodes compared to bone marrow and peripheral blood. *Leukemia*. 2017;31(6):1340-1347. doi:10.1038/leu.2017.11
4. Haselager MV, Kater AP, Eldering E. Proliferative signals in chronic lymphocytic leukemia; what are we missing? *Front Oncol*. 2020;10:592205. doi:10.3389/fonc.2020.592205
5. van Gent R, Kater AP, Otto SA, et al. In vivo dynamics of stable chronic lymphocytic leukemia inversely correlate with somatic hypermutation levels and suggest no major leukemic turnover in bone marrow. *Cancer Res*. 2008;68(24):10137-10144. doi:10.1158/0008-5472.CAN-08-2325
6. Guièze R, Liu VM, Rosebrock D, et al. Mitochondrial reprogramming underlies resistance to BCL-2 inhibition in lymphoid malignancies. *Cancer Cell*. 2019;36(4):369-384.e13. doi:10.1016/j.ccell.2019.08.005
7. Woyach JA, Ruppert AS, Heerema NA, et al. Ibrutinib regimens versus chemoimmunotherapy in older patients with untreated CLL. *N Engl J Med*. 2018;379(26):2517-2528. doi:10.1056/nejmoa1812836
8. van Attekum MH, Eldering E, Kater AP. Chronic lymphocytic leukemia cells are active participants in microenvironmental cross-talk. *Haematologica*. 2017;102(9):1469-1476. doi:10.3324/haematol.2016.142679
9. Burger JA, Wiestner A. Targeting B cell receptor signalling in cancer: preclinical and clinical advances. *Nat Rev Cancer*. 2018;18(3):148-167. doi:10.1038/nrc.2017.121
10. Burger JA, Ghia P, Rosenwald A, Caligaris-Cappio F. The microenvironment in mature B-cell malignancies: A target for new treatment strategies. *Blood*. 2009;114(16):3367-3375. doi:10.1182/blood-2009-06-225326
11. Pascutti MF, Jak M, Tromp JM, et al. IL-21 and CD40L signals from autologous T cells can induce antigen-independent proliferation of CLL cells. *Blood*. 2013;122(17):3010-3019. doi:10.1182/blood-2012-11-467670
12. Chen Z, Simon-Molas H, Cretenet G, et al. Characterization of metabolic alterations of chronic lymphocytic leukemia in the lymph node microenvironment. *Blood*. 2022;140:630-643. doi:10.1182/blood.2021013990
13. Schleiss C, Ilias W, Tahar O, et al. BCR-associated factors driving chronic lymphocytic leukemia cells proliferation ex vivo. *Sci Rep*. 2019;9(1):701. doi:10.1038/s41598-018-36853-8
14. Sun C, Chen YC, Martinez Zurita A, et al. The immune microenvironment shapes transcriptional and genetic heterogeneity in chronic lymphocytic leukemia. *Blood Adv*. 2023;7(1):145-158. doi:10.1182/bloodadvances.2021006941
15. Nadeu F, Royo R, Massoni-Badosa R, et al. Detection of early seeding of Richter transformation in chronic lymphocytic leukemia. *Nat Med*. 2022;28(8):1662-1671. doi:10.1038/s41591-022-01927-8
16. Knisbacher BA, Lin Z, Hahn CK, et al. Molecular map of chronic lymphocytic leukemia and its impact on outcome. *Nat Genet*. 2022;54(11):1664-1674. doi:10.1038/s41588-022-01140-w
17. Penter L, Gohil SH, Lareau C, et al. Longitudinal single-cell dynamics of chromatin accessibility and mitochondrial mutations in chronic lymphocytic leukemia mirror disease history. *Cancer Discovery*. 2021;11(12):3048-3063. doi:10.1158/2159-8290.CD-21-0276

18. Heinrich P, Kohler C, Ellmann L, et al. Correcting for natural isotope abundance and tracer impurity in MS-, MS/MS- and high-resolution-multiple-tracer-data from stable isotope labeling experiments with IsoCorrectoR. *Sci Rep*. 2018;8(1):17910. doi:10.1038/s41598-018-36293-4
19. Concordet JP, Haeussler M. CRISPOR: intuitive guide selection for CRISPR/Cas9 genome editing experiments and screens. *Nucleic Acids Res*. 2018;46(W1):W242-W245. doi:10.1093/nar/gky354
20. Haeussler M, Schönig K, Eckert H, et al. Evaluation of off-target and on-target scoring algorithms and integration into the guide RNA selection tool CRISPOR. *Genome Biol*. 2016;17(1):148. doi:10.1186/s13059-016-1012-2
21. Conant D, Hsiau T, Rossi N, et al. Inference of CRISPR Edits from Sanger Trace Data. *CRISPR J*. 2022;5(1):123-130. doi:10.1089/crispr.2021.0113
22. Vande Voorde J, Ackermann T, Pfetzer N, et al. Improving the metabolic fidelity of cancer models with a physiological cell culture medium. *Sci Adv*. 2019;5(1):eaau7314. doi:10.1126/sciadv.aau7314
23. Cantor JR, Abu-Remaileh M, Kanarek N, et al. Physiologic medium rewires cellular metabolism and reveals uric acid as an endogenous inhibitor of UMP synthase. *Cell*. 2017;169(2):258-272.e17. doi:10.1016/j.cell.2017.03.023
24. Simon-Molas H, Del Prete R, Kabanova A. Glucose metabolism in B cell malignancies: a focus on glycolysis branching pathways. *Mol Oncol*. 2024;18(7):1777-1794. doi:10.1002/1878-0261.13570
25. Calissano C, Damle RN, Marsilio S, et al. Intraclonal complexity in chronic lymphocytic leukemia: fractions enriched in recently born/divided and older/quiescent cells. *Mol Med*. 2011;17(11-12):1374-1382. doi:10.2119/MOLMED.2011.00360
26. Guo B, Zhang L, Chiorazzi N, Rothstein TL. IL-4 rescues surface IgM expression in chronic lymphocytic leukemia. *Blood*. 2016;128(4):553-562. doi:10.1182/blood-2015-11-682997
27. Mongini PKA, Gupta R, Boyle E, et al. TLR-9 and IL-15 synergy promotes the in vitro clonal expansion of chronic lymphocytic leukemia B cells. *J Immunol*. 2015;195(3):901-923. doi:10.4049/JIMMUNOL.1403189
28. Aguilar-Hernandez MM, Blunt MD, Dobson R, et al. IL-4 enhances expression and function of surface IgM in CLL cells. *Blood*. 2016;127(24):3015-3025. doi:10.1182/BLOOD-2015-11-682906
29. Gupta R, Li W, Yan XJ, et al. Mechanism for IL-15-driven B cell chronic lymphocytic leukemia cycling: roles for AKT and STAT5 in modulating cyclin D2 and DNA damage response proteins. *J Immunol*. 2019;202(10):2924-2944. doi:10.4049/JIMMUNOL.1801142
30. Leonard WJ, Lin JX, O'Shea JJ. The γ c family of cytokines: basic biology to therapeutic ramifications. *Immunity*. 2019;50(4):832-850. doi:10.1016/j.immuni.2019.03.028
31. Nardi F, Pezzella L, Drago R, et al. Assessing gene function in human B cells: CRISPR/Cas9-based gene editing and mRNA-based gene expression in healthy and tumor cells. *Eur J Immunol*. 2022;52(8):1362-1365. doi:10.1002/eji.202149784
32. Langbein S, Zerilli M, Zur Hausen A, et al. Expression of transketolase TKTL1 predicts colon and urothelial cancer patient survival: Warburg effect reinterpreted. *Br J Cancer*. 2006;94(4):578-585. doi:10.1038/sj.bjc.6602962
33. Tian WN, Braunstein LD, Pang J, et al. Importance of glucose-6-phosphate dehydrogenase activity for cell growth. *J Biol Chem*. 1998;273(17):10609-10617. doi:10.1074/jbc.273.17.10609
34. Boros LG, Torday JS, Lim S, Bassilian S, Cascante M, Lee WN. Transforming growth factor beta2 promotes glucose carbon incorporation into nucleic acid ribose through the nonoxidative pentose cycle in lung epithelial carcinoma cells. *Cancer Res*. 2000;60(5):1183-1185.
35. Cascante M, Centelles JJ, Veech RL, Lee WNP, Boros LG. Role of thiamin (vitamin B-1) and transketolase in tumor cell proliferation. *Nutr Cancer*. 2000;36(2):150-154. doi:10.1207/S15327914NC3602_2
36. Bichi R, Shinton SA, Martin ES, et al. Human chronic lymphocytic leukemia modeled in mouse by targeted *TCL1* expression. *Proc Natl Acad Sci USA*. 2002;99(10):6955-6960. doi:10.1073/pnas.102181599
37. Del Prete R, Drago R, Nardi F, et al. Robust and cost-effective CRISPR/Cas9 gene editing of primary tumor B cells in Eμ-TCL1 model of chronic lymphocytic leukemia. *HemaSphere*. 2024;8(8):e134. doi:10.1002/hem3.134
38. Chen Z, Cretenet G, Carnazzo V, et al. Electron transport chain and mTOR inhibition synergistically decrease CD40 signaling and counteract venetoclax resistance in chronic lymphocytic leukemia. *Haematologica*. 2024;109(1):151-162. doi:10.3324/haematol.2023.282760
39. Lu J, Cannizzaro E, Meier-Abt F, et al. Multi-omics reveals clinically relevant proliferative drive associated with mTOR-MYC-OXPHOS activity in chronic lymphocytic leukemia. *Nat Cancer*. 2021;2(8):853-864.
40. Li M, Zhao X, Yong H, et al. Transketolase promotes colorectal cancer metastasis through regulating AKT phosphorylation. *Cell Death Dis*. 2022;13(2):99. doi:10.1038/s41419-022-04575-5
41. Milne JV, Zhang BZ, Fujihara KM, Dawar S, Phillips WA, Clemons NJ. Transketolase regulates sensitivity to APR−246 in p53-null cells independently of oxidative stress modulation. *Sci Rep*. 2021;11(1):4480. doi:10.1038/s41598-021-83979-3
42. Qin Z, Xiang C, Zhong F, et al. Transketolase (TKT) activity and nuclear localization promote hepatocellular carcinoma in a metabolic and a non-metabolic manner. *J Exp Clin Cancer Res*. 2019;38(1):154. doi:10.1186/s13046-019-1131-1
43. Xu IMJ, Lai RKH, Lin SH, et al. Transketolase counteracts oxidative stress to drive cancer development. *Proc Natl Acad Sci USA*. 2016;113(6):E725-E734. doi:10.1073/pnas.1508779113
44. Tang YC, Hsiao JR, Jiang SS, et al. c-MYC-directed NRF2 drives malignant progression of head and neck cancer via glucose-6-phosphate dehydrogenase and transketolase activation. *Theranostics*. 2021;11(11):5232-5247. doi:10.7150/thno.53417
45. Zhen X, Zhang M, Hao S, Sun J. Glucose-6-phosphate dehydrogenase and transketolase: Key factors in breast cancer progression and therapy. *Biomed Pharmacother*. 2024;176:116935. doi:10.1016/j.biopha.2024.116935
46. Benito A, Polat IH, Noé V, Ciudad CJ, Marin S, Cascante M. Glucose-6-phosphate dehydrogenase and transketolase modulate breast cancer cell metabolic reprogramming and correlate with poor patient outcome. *Oncotarget*. 2017;8(63):106693-106706. doi:10.18632/oncotarget.21601
47. Ahmad F, Dixit D, Sharma V, et al. Nrf2-driven TERT regulates pentose phosphate pathway in glioblastoma. *Cell Death Dis*. 2016;7:e2213. doi:10.1038/cddis.2016.117
48. Saha A, Connelly S, Jiang J, et al. Akt phosphorylation and regulation of transketolase is a nodal point for amino acid control of purine synthesis. *Mol Cell*. 2014;55(2):264-276. doi:10.1016/j.molcel.2014.05.028
49. Bunik VI, Tylicki A, Lukashev NV. Thiamin diphosphate-dependent enzymes: from enzymology to metabolic regulation, drug design and disease models. *FEBS J*. 2013;280(24):6412-6442. doi:10.1111/febs.12512
50. Jia D, Liu C, Zhu Z, et al. Novel transketolase inhibitor oroxylin A suppresses the non-oxidative pentose phosphate pathway and hepatocellular carcinoma tumour growth in mice and patient-derived organoids. *Clin Transl Med*. 2022;12(11):e1095. doi:10.1002/ctm2.1095
51. Xiao G, Chan LN, Klemm L, et al. B-Cell-specific diversion of glucose carbon utilization reveals a unique vulnerability in B cell malignancies. *Cell*. 2018;173(2):470-484.e18. doi:10.1016/j.cell.2018.02.048
52. Mitsuishi Y, Taguchi K, Kawatani Y, et al. Nrf2 redirects glucose and glutamine into anabolic pathways in metabolic reprogramming. *Cancer Cell*. 2012;22(1):66-79. doi:10.1016/j.ccr.2012.05.016
53. Hoferkova E, Seda V, Kadakova S, et al. Stromal cells engineered to express T cell factors induce robust CLL cell proliferation in vitro and

in PDX co-transplantations allowing the identification of RAF inhibitors as anti-proliferative drugs. *Leukemia*. 2024;38(8):1699-1711. doi:10.1038/s41375-024-02284-w

54. Touw I, Dorssers L, Lowenberg B. The proliferative response of B cell chronic lymphocytic leukemia to interleukin 2: functional characterization of the interleukin 2 membrane receptors. *Blood*. 1987;69(6):1667-1673. doi:10.1182/blood.V69.6.1667.1667
55. Hazan-Halevy I, Harris D, Liu Z, et al. STAT3 is constitutively phosphorylated on serine 727 residues, binds DNA, and activates transcription in CLL cells. *Blood*. 2010;115(14):2852-2863. doi:10.1182/blood-2009-10-230060
56. Kondo K, Shaim H, Thompson PA, et al. Ibrutinib modulates the immunosuppressive CLL microenvironment through STAT3-mediated suppression of regulatory B-cell function and inhibition of the PD-1/PD-L1 pathway. *Leukemia*. 2018;32(4):960-970. doi:10.1038/leu.2017.304
57. Rozovski U, Veletic I, Harris DM, et al. STAT3 activates the pentraxin 3 gene in chronic lymphocytic leukemia cells. *J Immunol*. 2022;208(12):2847-2855. doi:10.4049/jimmunol.2101105
58. Brown JR, Walker SR, Heppler LN, et al. Targeting constitutively active STAT3 in chronic lymphocytic leukemia: A clinical trial of the STAT3 inhibitor pyrimethamine with pharmacodynamic analyses. *Am J Hematol*. 2021;96(4):E95-E98. doi:10.1002/ajh.26084
59. Wegrzyn J, Potla R, Chwae YJ, et al. Function of mitochondrial Stat3 in cellular respiration. *Science (New York, N.Y.)*. 2009;323(5915):793-797. doi:10.1126/science.1164551
60. Balic JJ, Albargy H, Luu K, et al. STAT3 serine phosphorylation is required for TLR4 metabolic reprogramming and IL-1β expression. *Nat Commun*. 2020;11(1):3816. doi:10.1038/s41467-020-17669-5
61. Patel SB, Nemkov T, Stefanoni D, et al. Metabolic alterations mediated by STAT3 promotes drug persistence in CML. *Leukemia*. 2021;35(12):3371-3382. doi:10.1038/s41375-021-01315-0